Defense Threat Reduction Agency
8725 John J. Kingman Road, MS-6201
Fort Belvoir, VA 22060-6201

DTRA-TR-16-058

TECHNICAL REPORT

Models of Hemodynamics and Hematopoiesis Following Hemorrhage for Use in Combined Injury Simulations

June 2016

HDTRA1-14-D-0003; 0005

Prepared by:

Applied Research Associates, Inc.
801 N. Quincy Street
Suite 700
Arlington, VA 22203

This page intentionally left blank.

REPORT DOCUMENTATION PAGE

Form Approved
OMB No. 0704-0188

PLEASE DO NOT RETURN YOUR FORM TO THE ABOVE ADDRESS.

1. REPORT DATE *(DD-MM-YYYY)*	2. REPORT TYPE	3. DATES COVERED *(From - To)*
30-06-2016	Technical Report	

4. TITLE AND SUBTITLE

Models of Hemodynamics and Hematopoiesis Following Hemorrhage for Use in Combined Injury Simulations

5a. CONTRACT NUMBER

HDTRA1-14-D-0003/0005

5b. GRANT NUMBER

5c. PROGRAM ELEMENT NUMBER

6. AUTHOR(S)

Bellman, Jacob
Crary, David
Stricklin, Daniela

5d. PROJECT NUMBER

5e. TASK NUMBER

5f. WORK UNIT NUMBER

7. PERFORMING ORGANIZATION NAME(S) AND ADDRESS(ES)

Applied Research Associates, Inc.
801 N. Quincy Street, Suite 700
Arlington, VA 22203

8. PERFORMING ORGANIZATION REPORT NUMBER

9. SPONSORING/MONITORING AGENCY NAME(S) AND ADDRESS(ES)

Nuclear Technologies Department, Attn: Dr. Blake
Defense Threat Reduction Agency
8725 John J. Kingman Road, Mail Stop 6201
Fort Belvoir, VA 22060-6201

10. SPONSOR/MONITOR'S ACRONYM(S)

DTRA J9NTSN

11. SPONSOR/MONITOR'S REPORT NUMBER(S)

DTRA-TR-16-058

12. DISTRIBUTION/AVAILABILITY STATEMENT

DISTRIBUTION A. Approved for public release: distribution is unlimited.

13. SUPPLEMENTARY NOTES

14. ABSTRACT

This report describes inclusion of the effects of hemorrhage in previously developed models that simulate hemodynamics and hematopoiesis in humans. In each of these systems, hemorrhage induces loss of a component in circulation. In the granulopoiesis model, there is an additional response of demargination, which releases a subset of granulocytes in the blood vessels into circulation, causing an upsurge of granulocytes in blood plasma. Each hematopoietic model has been developed to simulate humans and mice, and the models have been compared to the available data. The fluid dynamics and thrombopoiesis models have been validated against existing data, whereas there is no available data to validate the human granulopoiesis model. Simulations of the murine hematopoietic models verify that the models compare well to combined radiation and hemorrhage data. These models will aid in the prediction of 48-hour and 60-day lethality of combined injury resulting from a nuclear detonation and will assist in medical planning.

15. SUBJECT TERMS

Hemorrhage, Combined Injury, Ordinary Differential Equation Model, Fluid Redistribution, Thrombopoiesis, Granulopoiesis, Lymphopoiesis

16. SECURITY CLASSIFICATION OF:			17. LIMITATION OF ABSTRACT	18. NUMBER OF PAGES	19a. NAME OF RESPONSIBLE PERSON
a. REPORT	b. ABSTRACT	c. THIS PAGE			Dr. Paul Blake, Ph.D.
U	U	U	U	62	19b. TELEPHONE NUMBER *(Include area code)* 703-767-3433

UNIT CONVERSION TABLE

U.S. customary units to and from international units of measurement*

U.S. Customary Units	Multiply by → / ← Divide by†		International Units
Length/Area/Volume			
inch (in)	2.54	$\times 10^{-2}$	meter (m)
foot (ft)	3.048	$\times 10^{-1}$	meter (m)
yard (yd)	9.144	$\times 10^{-1}$	meter (m)
mile (mi, international)	1.609 344	$\times 10^{3}$	meter (m)
mile (nmi, nautical, U.S.)	1.852	$\times 10^{3}$	meter (m)
barn (b)	1	$\times 10^{-28}$	square meter (m^2)
gallon (gal, U.S. liquid)	3.785 412	$\times 10^{-3}$	cubic meter (m^3)
cubic foot (ft^3)	2.831 685	$\times 10^{-2}$	cubic meter (m^3)
Mass/Density			
pound (lb)	4.535 924	$\times 10^{-1}$	kilogram (kg)
atomic mass unit (AMU)	1.660 539	$\times 10^{-27}$	kilogram (kg)
pound-mass per cubic foot ($lb\ ft^{-3}$)	1.601 846	$\times 10^{1}$	kilogram per cubic meter ($kg\ m^{-3}$)
Pound-force (lbf avoirdupois)	4.448 222		Newton (N)
Energy/Work/Power			
electron volt (eV)	1.602 177	$\times 10^{-19}$	joule (J)
erg	1	$\times 10^{-7}$	joule (J)
kiloton (kT) (TNT equivalent)	4.184	$\times 10^{12}$	joule (J)
British thermal unit (Btu) (thermochemical)	1.054 350	$\times 10^{3}$	joule (J)
foot-pound-force (ft lbf)	1.355 818		joule (J)
calorie (cal) (thermochemical)	4.184		joule (J)
Pressure			
atmosphere (atm)	1.013 250	$\times 10^{5}$	pascal (Pa)
pound force per square inch (psi)	6.984 757	$\times 10^{3}$	pascal (Pa)
Temperature			
degree Fahrenheit (°F)	[T(°F) − 32]/1.8		degree Celsius (°C)
degree Fahrenheit (°F)	[T(°F) + 459.67]/1.8		kelvin (K)
Radiation			
activity of radionuclides [curie (Ci)]	3.7	$\times 10^{10}$	per second (s^{-1}‡)
air exposure [roentgen (R)]	2.579 760	$\times 10^{-4}$	coulomb per kilogram ($C\ kg^{-1}$)
absorbed dose (rad)	1	$\times 10^{-2}$	joule per kilogram ($J\ kg^{-1}$§)
equivalent and effective dose (rem)	1	$\times 10^{-2}$	joule per kilogram ($J\ kg^{-1}$**)

*Specific details regarding the implementation of SI units may be viewed at http://www.bipm.org/en/si/.

†Multiply the U.S. customary unit by the factor to get the international unit. Divide the international unit by the factor to get the U.S. customary unit.

‡The special name for the SI unit of the activity of a radionuclide is the becquerel (Bq). ($1\ Bq = 1\ s^{-1}$).

§The special name for the SI unit of absorbed dose is the gray (Gy). ($1\ Gy = 1\ J\ kg^{-1}$).

**The special name for the SI unit of equivalent and effective dose is the sievert (Sv). ($1\ Sv = 1\ J\ kg^{-1}$).

Table of Contents

Table of Contents i
List of Figures iii
List of Tables v
Acknowledgements vi
Executive Summary 1
Section 1. Introduction 2
1.1 Background 2
1.2 Approach 2
Section 2. Hemodynamics after Hemorrhage 3
2.1 Hemorrhagic Shock in the Context of Thermal Injury 3
2.2 Review of the Understanding of Hemorrhage and its Effects 4
2.2.1. Experimental Studies with Humans and Animal Models 4
2.2.2. Computer Models of Hemorrhage 5
2.3 Modeling Hemorrhage in the CSM 7
2.3.1. Methods 7
2.3.2. CSM Results 9
Section 3. Hematopoiesis After Hemorrhage 11
3.1 Background 11
3.1.1. General Hematopoiesis 11
3.1.2. Method for Integrating Hemorrhage 12
3.2 Thrombopoiesis Model 13
3.3 Granulopoiesis Model 16
3.3.1. Granulocyte Demargination 17
3.3.2. Granulocyte Cell Kinetics following Radiation 18
3.3.3. Granulocyte Cell Kinetics following Hemorrhage 19
3.4 Lymphopoiesis Model 19
3.5 Modeling Combined Hemorrhage and Radiation 22
3.6 Discussion 24
Section 4. Summary 25

4.1 Models to date 25
4.2 Future work 25
4.2.1. Model Improvements and Additional Validation 25
4.2.2. Other Mechanistic Models 25
4.2.3. Mapping Model Outputs to Predicting Risk of Outcomes 26
Section 5. References 27
Section 6. Abbreviations, Acronyms and Symbols 32
Appendix A. Supplemental Tables 33
Appendix B. Supplemental Figures 38
B-1. Human Thrombocytapheresis Experiments 38
B-2. Human Radiation-Induced Granulocyte Demargination 40
B-3. Murine Radiation-Induced Granulocyte Demargination 49

List of Figures

Figure 1. Compartmental model of microvascular exchange for thermal injury (Ampratwum et al. 1995) 8
Figure 2. Plasma volume as a function of time for 10% hemorrhage of 15-minute duration 10
Figure 3. Diagram of the generic hematopoietic model structure 12
Figure 4. Diagram of the thrombopoiesis model structure 14
Figure 5. Simulation of plateletpheresis (Lasky et al. 1981) with the thrombopoiesis model 15
Figure 6. Simulation of plateletpheresis (Sullivan et al. 1977) with the thrombopoiesis model .. 16
Figure 7. Diagram of the granulopoiesis model structure 17
Figure 8. Radiation-induced demargination of granulocytes 18
Figure 9. Murine neutrophil data (Gaylor et al. 1969) following hemorrhage 19
Figure 10. Diagram of the lymphopoiesis model structure 20
Figure 11. Lymphocytes following hemorrhage 21
Figure 12. Experimental data of swine lymphocyte response to hemorrhage 21
Figure 13. Murine hematopoietic response to combined radiation and burn injuries 23
Figure B-1. Simulation of a human TP study (Dettke 1998) with the thrombopoiesis model 38
Figure B-2. Simulation of a human TP study (Fontana 2011) with the thrombopoiesis model ... 38
Figure B-3. Simulation of a human TP study (Stohlawetz 1998) with the thrombopoiesis model 39
Figure B-4. Simulation of a human TP study (Weisbach 1999) with the thrombopoiesis model 39
Figure B-5. Human granulocyte data used for optimization of radiation-induced demargination parameters (1 of 4) 40
Figure B-6. Human granulocyte data used for optimization of radiation-induced demargination parameters (2 of 4) 41
Figure B-7. Human granulocyte data used for optimization of radiation-induced demargination parameters (3 of 4) 42
Figure B-8. Human granulocyte data used for optimization of radiation-induced demargination parameters (4 of 4) 43
Figure B-9. Human granulocyte data used for validation of radiation-induced demargination parameters (1 of 5) 44
Figure B-10. Human granulocyte data used for validation of radiation-induced demargination parameters (2 of 5) 45

Figure B-11. Human granulocyte data used for validation of radiation-induced demargination parameters (3 of 5) 46
Figure B-12. Human granulocyte data used for validation of radiation-induced demargination parameters (4 of 5) 47
Figure B-13. Human granulocyte data used for validation of radiation-induced demargination parameters (5 of 5) 48
Figure B-14. Murine granulocyte data used for optimization of radiation-induced demargination parameters (1 of 4) 49
Figure B-15. Murine granulocyte data used for optimization of radiation-induced demargination parameters (2 of 4) 50
Figure B-16. Murine granulocyte data used for optimization of radiation-induced demargination parameters (3 of 4) 51
Figure B-17. Murine granulocyte data used for optimization of radiation-induced demargination parameters (4 of 4) 52

List of Tables

Table 1: Computer Models of Hemorrhage 6
Table A-1. Human Thrombocytapheresis Data 33
Table A-2. Radiation-Induced Granulocyte Demargination Parameters 33
Table A-3. Hemorrhage-Induced Granulocyte Demargination Parameters 34
Table A-4. Human Optimization Data for Radiation-Induced Granulocyte Demargination 35
Table A-5. Human Validation Data for Radiation-Induced Granulocyte Demargination 36
Table A-6. Murine Optimization Data for Radiation-Induced Granulocyte Data 37

Acknowledgements

The modeling work presented in this report was built on decades of detailed and thoughtful experimental research from a variety of scientific communities. The authors gratefully acknowledge the technical developments and/or support of the following individuals: Dr. Olga Smirnova, Dr. Joel L. Bert, Dr. R.T. Ampratwum, Ms. Jacqueline Wentz, and the many experimentalists who produced the data against which our models are compared.

We also gratefully acknowledge Dr. Paul Blake of DTRA/J9 for programmatic support. The work was performed under DTRA contract HDTRA1-14-D-0003; 005.

Executive Summary

As part of the ongoing effort to develop a suite of predictive biomathematical tools for the analysis of combined injury effects caused by a nuclear detonation, computer models of hemodynamics (fluid redistribution) and hematopoiesis (blood cell dynamics) have been developed and integrated into a health effects modeling platform, HENRE (Health Effects from Nuclear and Radiological Environments). These models were initially developed in the context of radiation and thermal injury. The following technical report describes the extension of these models to include the effects of hemorrhage. These extensions are the first step to include the effects of blast trauma in HENRE in combination with radiation and burn injury.

The extensions include:

- A fluid loss term in the Coupled Starling Model (CSM) of hemodynamics. This provides an estimation of plasma volume as a function of time during and after hemorrhage, which is a key component for predicting the risk of circulatory shock and probability of lethality in the first 48 hours after injury.
- Accounting for blood cell loss in the dynamics of thrombocytes, granulocytes, and lymphocytes after hemorrhage. For the granulopoiesis model, the effects of demargination were included in the context of radiation and hemorrhage. The dynamics of these hemocytes are important in determining the time course of injury, particularly the delayed risks of internal hemorrhage and infection, and long term (60-day) lethality.

Some results from this modeling effort are:

- The thrombocyte model and the CSM with hemorrhage effects included compare well to available data.
- A finding that the lack of human data is a problem for the development of the granulocyte and lymphocyte models.
    - Development of a murine model, which compares well to data, has facilitated in human parameter extrapolation for the granulocyte model, but the model still requires additional data for validation.
    - The lymphocyte model is unable to reproduce an upsurge in lymphocyte number seen in the data immediately after hemorrhage, an effect which is not clearly understood in the literature.

It is important to have a strong understanding of time-dependent dynamics of each of these systems. Computer models can help predict the extent of individual injury, aid in the risk-assessment of mortality, and determine timing/extent of fluid therapy required for rehabilitation. A large scale nuclear event can be expected to result in many casualties with various combinations of injuries. Computer models can help predict the resource requirements for attending to casualties and assist in medical planning. Model extensions described in this report will be added to the latest version of HENRE, and these models will continue to be improved.

Section 1.

Introduction

1.1 Background

As part of its mission to safeguard against weapons of mass destruction (WMD), the Defense Threat Reduction Agency (DTRA) supports the development of capabilities to reduce, eliminate and counter WMD threats and mitigate their effects. Applied Research Associates, Inc. (ARA) has supported DTRA's mission by developing state-of-the-art mathematical models that predict medical and human performance consequences from ionizing radiation exposure and combined injuries, thereby enhancing our understanding of the potential impact of a nuclear detonation. We have improved current casualty estimation capabilities through an interdisciplinary approach that integrates experimental data with mechanistic mathematical modeling.

A nuclear detonation scenario would result in large numbers of casualties involving radiation, thermal, and blast injuries. Our current modeling effort has been focused on mechanistic models that estimate the impact of both individual and combined injuries. Using a mechanistic approach to understand the impact of individual insults allows us to account for combined action among the injury processes. The use of mechanistic models also provides valuable insight into the time course of injuries. Previously, we have developed a series of models that examine the impact of radiation and thermal burn as two separate mechanistic processes. However, another major impact of nuclear weapons is blast-related effects. A number of traumatic injuries can result including lacerations, broken bones, contusions, crush injuries, and hemorrhage. Hemorrhage, for one, can dramatically impact survivability. Therefore, the current effort focuses on estimating the impact of hemorrhage on the key mechanistic models under investigation.

1.2 Approach

Prior to the current work, mechanistic models for two primary systems were implemented in the Health Effects from Nuclear and Radiological Environments (HENRE) computer modeling platform:

- For the hemodynamic system, the Coupled Starling Model (CSM) estimates blood fluid dynamics after radiation and thermal injury. One key output of the model (plasma volume) is used to extrapolate to risk of circulatory shock and probability of lethality in the first 48 hours after injury.
- For the hematopoietic system, three separate models estimate the dynamics of thrombocytes, granulocytes, and lymphocytes after radiation and thermal injury. The outputs of these models provide insight into time course of injury and delayed risks such as internal hemorrhage and infection. These models can be used to estimate 60-day lethality.

The current work builds on these existing models by incorporating hemorrhage. Below, we describe how hemorrhage is incorporated in each model, and how hemorrhage effects the response and recovery of each system.

Section 2.

Hemodynamics after Hemorrhage

As described above, the overall purpose of this work is to incorporate hemorrhage into our mechanistic models of nuclear blast effects, with the ultimate goal of correlating plasma volume and hematopoietic variables with the risk of serious injury and mortality. While hemorrhage alone directly redistributes fluid volumes as a result of the physiological response to loss of plasma and red blood cells, response to both thermal and radiation insults also redistributes fluids in a manner that competes with and reinforces the effects of hemorrhage.

The first subsection below gives a brief review of hemodynamic effects of thermal injury leading to hemorrhagic shock and possible death. The second subsection reviews understanding of hemorrhage from experiments and from computer modeling leading to recommendation of the CSM for incorporating the effects of hemorrhage on hemodynamics in HENRE. The final subsection describes the use of the CSM for this purpose.

2.1 Hemorrhagic Shock in the Context of Thermal Injury

Thermal injury causes a series of interrelated events within a short period of time, resulting in a risk of burn shock (Latenser 2009; Williams 2009). Burn shock is a combination of several circulatory abnormalities which include distributive shock, hypovolemic shock, and cardiogenic shock (Shaw 1994). Circulating blood volume lost to the interstitial space leads to hypovolemia, which can occur with burn injuries involving 15% total body surface area (TBSA) or more. Edema, which plays a critical role in the pathophysiological process of burn shock, begins immediately after injury and resolves after about 48 hours. Edema refers to the accumulation of fluid in the interstitial space of tissues, which contributes to the loss of circulating fluid volume and increased pressure in the affected tissues. Edema can be observed even at sites distant from the burned area in cases of about 20% TBSA or more, due to underlying systemic mediator-related mechanisms. Although edema is a natural process in wound healing, it can cause complications after injury if it impairs tissue perfusion. In the affected area, the dramatic increase in interstitial fluid volume and increased pressures lead to damage of the interstitial structure due to denaturation and unraveling of connective tissue collagen fibers. Intra-vasculature fluid loss contributes to evolution of shock.

The microcirculation in the injured area causes blood vessels to lose integrity. Proteins are lost into the interstitial space, which causes the intravascular colloid osmotic pressure to dramatically drop. Fluid is further released from circulation and a transient decrease in interstitial pressure results from the release of osmotically active particles. This process creates a suction which pulls fluid from the plasma space. A dramatic fluid flux into the interstitial space collectively results from decreased interstitial pressures, increased capillary permeability that results from circulating mediators, and an imbalance in hydrostatic and oncotic pressures. Fluid, electrolytes, and proteins then equilibrate between the intravascular and interstitial space (Latenser 2009; Williams 2009).

Although a number of additional mechanisms are involved in the increase in risk of circulatory shock (Pham et al. 2008), we identified the early permeability changes and fluid shifts resulting from thermal and radiation as key mechanisms for our modeling purposes (Stricklin 2013).

The following section provides an overview of current understanding and existing models of hemorrhage and the rationale for selecting a computer model for incorporation into ARA's Health Effects from Nuclear and Radiological Environments (HENRE) platform for study of hemorrhage and hemorrhagic shock.

2.2 Review of the Understanding of Hemorrhage and its Effects

The following two subsections review the understanding of hemorrhage and its effects derived from experimental studies and from computer modeling, respectively.

2.2.1. Experimental Studies with Humans and Animal Models

The number of controlled experimental studies of hemorrhage in humans is somewhat limited. Many of the studies that exist have been undertaken for the purposes of studying the response to fluid therapy after hemorrhage (or of hypervolemic response), and do not focus on the physiological response to hemorrhage *per se*. The introduction of therapeutic fluids in these experiments generally occurs within 2 hours after hemorrhage, and masks the redistribution of solutes and fluids that is purely the result of the hemorrhage itself. Because of the dangers inherent in studies of large volume hemorrhage or hemorrhagic shock, animal models have been used in many experiments.

Traditionally, splenectomized dogs are the preferred animals in the design of experimental hemorrhagic shock models (Fülöp et al. 2013). The dogs must be splenectomized to allow for the extrapolation of results from canine experiments to humans because of a peculiarity of the canine physiology. During hemorrhage, the canine spleen contracts and forces red blood cells into the bloodstream, thus increasing hematocrit, blood volume, and changing other cardiovascular parameters. This dramatically increases the canine cardiovascular response, and in particular makes the hemorrhagic shock response in dogs highly variable. The splenic release of red blood cells as a response to hemorrhage is negligible in humans (Kemming et al. 2004). For splenectomized dog models, the assumption is that the response in humans can be recovered by scaling the response by the ratio of the respective fluid volumes between dogs and humans (Bert et al. 2000).

Studies in dogs have allowed hemorrhage to be studied over a wider range of volumes (as a fraction of total blood volume) than is available in human studies. Typically, hemorrhage of between 15% and 30% of total blood volume is called a 'moderate' hemorrhage, while those greater than 30% (which carry increased risk of hemorrhagic shock) are called 'large' (Gyenge et al. 2003). For blood loss less than approximately 15%, plasma refill and recovery of hemodynamic variables can be expected even in the absence of adjuvant fluid therapy. For larger hemorrhage, up to approximately 30% blood loss, compensatory mechanisms provide partial recovery, but without fluid therapy, hypovolemic shock will result. For blood loss greater than 35%, hemorrhagic shock will ensue even with the compensatory mechanisms active and with external fluid therapy.

One result that appears to be experimentally well-established is that during the initial phase of hemorrhage the blood volume restoration is dominated by the reduction of capillary pressure and subsequent refill of plasma from the interstitial spaces. By the use of both human and dog models this effect has been verified over a large range of hemorrhage volumes, from 10% to 40% (Gann et al. 1981). This is the classic Starling mechanism; a fall in capillary hydrostatic pressure promotes a shift in plasma from the interstitium into the circulation via the capillaries. From studies in both humans and dogs this initial phase of rapid refill of protein-free fluids lasts

for several hours and accounts for a significant restoration (25 – 50%) of plasma volume to pre-hemorrhage levels.

A second phase, which temporally overlaps with the first phase, involves the restitution of plasma proteins to support plasma oncotic pressure and continued blood volume expansion. While this increase in proteins has been well-established experimentally, the actual mechanism by which this occurs has not been definitively resolved. While investigators have concluded that return of protein from the interstitium via the lymphatic system plays an important role, there is a consensus that this mechanism does not provide the levels of albumin observed experimentally at all hemorrhage volumes. Therefore, other mechanisms have been investigated. These include increased fluid return during hemorrhage via the lymphatics (Cope and Litwin 1962), return of protein through hepatic or mesenteric capillaries (Lister et al. 1963), fluid shifts from cells to the interstitium (Pirkle and Gann 1975), the role of glucose and small solutes, and, for large hemorrhage, changes to the function of the Na^+-K^+ pump (Carlson et al. 1996).

Unlike the initial phase of blood volume restitution, the second phase shows significant dependence on volume of hemorrhage. Gann et al. (1981) have shown that in dogs the rate of protein restitution in moderate hemorrhage increases approximately linearly with hemorrhage volume up to a volume of approximately 25%. After this value the response is highly variable. Several mechanisms have been proposed to account for these effects, but these explanations remain a subject of debate.

Finally, it should be stressed that experimental studies almost always involve rapid hemorrhage, and the rate of hemorrhage is considered constant. For prolonged hemorrhage, the bleeding rate is not constant but proportional to mean arterial pressure. However, for comparison with experimental data, a constant flow rate is a reasonable approximation.

2.2.2. Computer Models of Hemorrhage

Table 1 shows a number of computer (*in silico*) models of hemorrhage. Other such models exist which describe clinical fluid volume disturbances. However, upon review, these were considered as not sufficiently detailed or tailored for specific applications, such as fluid resuscitation or renal dialysis, and were therefore not included in this list.

The second column in Table 1 indicates the animal model used in the development of the computer model parameters and/or comparison with data. The third column gives the additional features of the model beyond the Starling mechanism described above. The differing features in these models are attempts to incorporate additional mechanisms to increase plasma osmolarity and refill rates to that observed during the second phase.

The most comprehensive model to date is that of Gyenge et al. 2003. Their goal was to model blood volume restitution and plasma osmolarity for moderate to large hemorrhage, based on hemorrhage experiments on dogs. The model uses an empirical fit to data to provide analytical expressions for glucose and small solute release approximately two hours after hemorrhage. A parameter is used to account for decreased cellular exchange of small ions due to decreased Na^+-K^+ pump rate for large hemorrhage. In addition, the effects of solute and ion exchange with red blood cells are included, as well as fluid loss via the kidney. This model provides a good fit to data for hemorrhage from 10% to 30%, for both the rapid refill at short times, and the more gradual increase during the second phase of blood volume restitution.

Table 1: Computer Models of Hemorrhage

Reference	Model	Features
Pirkle & Gann 1975	Dog	Uses empirical model of lymphatic flow and arterial pressure as a function of blood volume
Mazzoni et al. 1988	Rabbit	Interstitial compliance, model of fluid shifts from red blood cells and endothelium, pore/conductivity model of endothelial membrane
Barnea & Sheffer 1993	Dog	Small solutes, blood vessel compliance
Carlson et al. 1996	Dog	3 compartments (intercellular, interstitial, intravascular), models exchange of small ions from binding sites on the interstitial proteoglycans (interstitial matrix), inhibition of Na^+-K^+-ATPase reaction
Bert et al. 2000	Human	4 compartments (interstitial cells, interstitial fluid, plasma, red blood cells)
Gyenge et al. 2003	Dog	4 compartments (interstitial cells, interstitial fluid, plasma, red blood cells) includes fluid and ion losses to kidney, empirical models for glucose and small ion release

Gyenge et al. 2003 showed the relative effect of blood volume restitution due to hydrostatic pressure and protein return via the lymphatics only, compared with this same mechanism plus small ion solute release. This effect is dependent on degree of hemorrhage. At 10% hemorrhage, the solutes account for approximately 40% of the total volume restitution at times greater than 2 hours, while for 30% this value decreases to about 25%.

Currently there is no general consensus on the precise mechanism of solute release, and the existing models are based on parameters derived from animal data. Unlike parameters such as blood volume, there is much greater uncertainty in scaling these parameters between species, as reflected in the continued controversy over the application and timing of fluid and hormones to be used in therapy for hypovolemia (Drucker et al. 1981). As a result, we have taken a pragmatic approach to modeling hemorrhage for the purpose of this study, and only included effects that are well understood to update the HENRE platform. This has led us to modify the existing HENRE CSM in a straightforward way. In this model, oncotic pressure is controlled by the protein (albumin) levels in the plasma and interstitium, and protein return to the plasma volume is via the lymphatic system. Effects due to small ion release, glucose, etc., are not considered.

The CSM, discussed previously (Oldson et al. 2015; Stricklin and Oldson 2015) and described below, provides a platform for simulating combined injury (radiation and thermal injury) based on well-established physiological principles. The way in which hemorrhage has been added to this model is described below.

2.3 Modeling Hemorrhage in the CSM

The CSM referenced here is a computer model of microvasculature exchange that describes the dramatic fluid shifts that occur after thermal injury, which can lead to burn shock (Ampratwum et al. 1995). The microvascular exchange model shown in Figure 1 describes the redistribution of fluid and albumin between three compartments: circulation, thermally injured interstitial tissue, and uninjured interstitial tissue. The model was later adapted to account for the immediate effects of radiation on vascular permeability to estimate the impact of combined injury (Oldson et al. 2015; Stricklin and Oldson 2015). Since both thermal injury and radiation parameters exist for this model, we selected this model to incorporate the effect of hemorrhage. As discussed above, while other models of hemorrhage exist, some of which take into account additional mechanistic detail specifically for hemorrhage (Doherty 1993; Gyenge et al. 2003; Torres et al. 2009; Reisner and Heldt 2013), these models have not been designed to account for the thermal injury and radiation. If more detailed approaches are necessary in the future, these alternative models can be explored further.

2.3.1. Methods

The CSM includes a parameter, J_{blood}, which was originally defined as the rate of plasma lost (in mL/h) due to escharotomies/fasciotomies (incisions to relieve pressure from fluid buildup), blood samples, and other procedures. We have tested the use of J_{blood} for parameterizing plasma lost to hemorrhage and compared the CSM results with available data. The plasma loss parameter, J_{blood}, appears in the CSM as a time-dependent source term in the rate equation for plasma volume. This parameter is coupled with the rate of blood albumin loss, $\dot{Q}_{blood}$, via a proportionality constant (the ratio of the blood albumin level and the plasma volume), but is not coupled directly with other quantities in the rate equations.

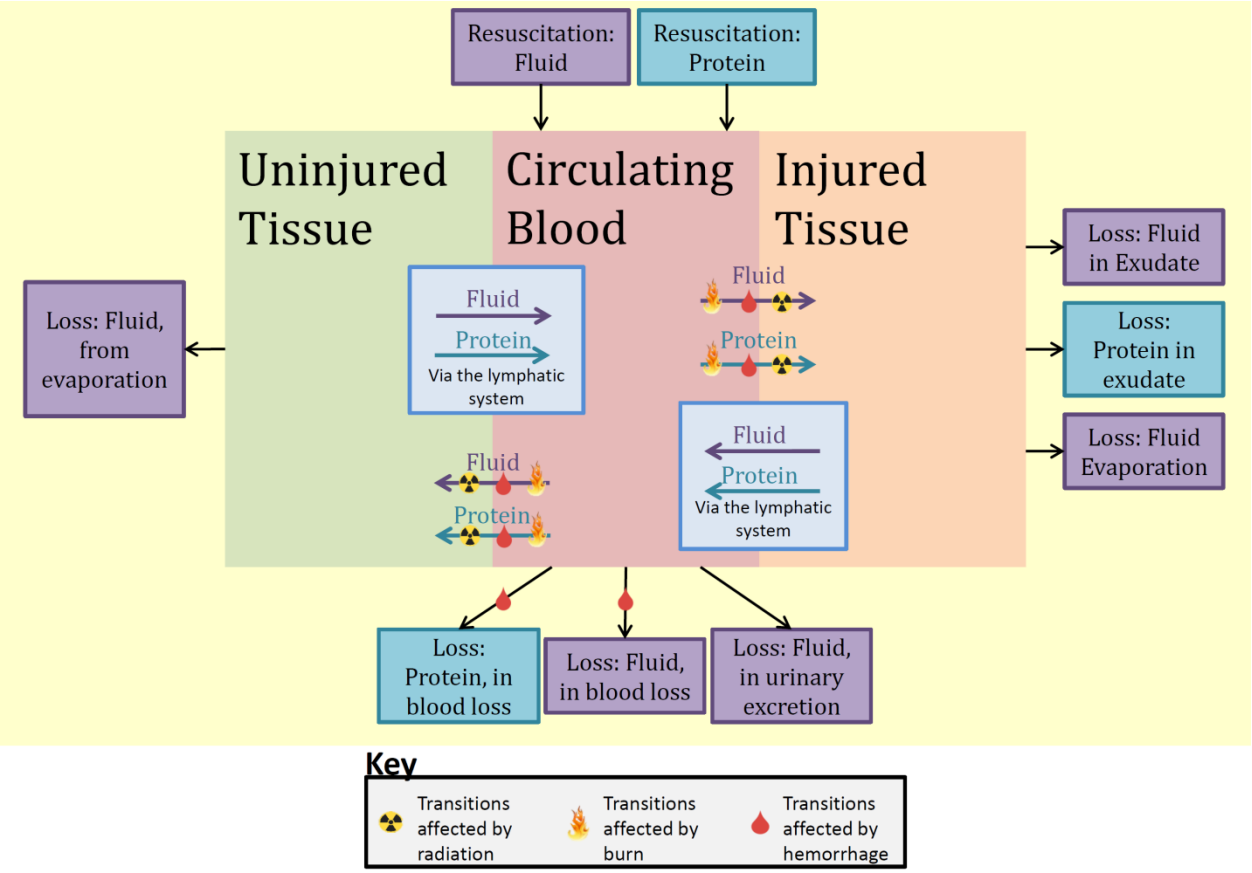

Figure 1. Compartmental model of microvascular exchange for thermal injury (Ampratwum et al. 1995)

To test the use of the J_{blood} parameter for defining plasma loss from hemorrhage, we have assumed that the time dependence of the rate, J_{blood}, is constant over the time of hemorrhage. The computer program of the CSM has been modified so the user is able to define a total blood plasma volume lost, V_h, as a percentage of total blood, and a duration, t_d (in hours), over which the hemorrhage occurs. In the CSM, J_{blood} is then defined as:

$$J_{blood} = \begin{cases} \dfrac{3200V_h}{t_d}, & 0 < t \leq t_d \\ 0, & t_d = 0; t > t_d \end{cases} \quad (1)$$

In Equation (1), the factor of 3200 represents the total plasma volume (in mL), and the percentage of blood lost is assumed equal to the plasma lost during the hemorrhage (Ampratwum et al. 1995). This latter assumption is valid when t_d is much smaller than the time scale associated with transcapillary refill, which is certainly the case for $t_d \leq 0.5$ hours.

To test these changes in the CSM, we performed hemorrhage calculations using the CSM, and the values for t_d and V_h from the study by Tølløfsrud et al. 1998, described below. The CSM results for plasma volume as a function of time were then compared with the results of this study and the model calculations of Bert et al. 2000. CSM calculations were done both with and without fluid resuscitation, though data is only available for the case of no fluid resuscitation.

Studies on the redistribution of blood components during hypovolemia are relatively few. The most recent source for data on plasma volume after hemorrhage is Tølløfsrud et al. 1998. In this study, nine volunteers were subjected to 10% blood loss over a period of 15 minutes, and the hemodynamic effects were recorded 90 minutes after the start of the hemorrhage. The main purpose of this study was to determine the effects of infusion of hypertonic saline and dextran on hemodynamics, and the fluid shifts between the interstitial and vascular spaces. The infusion was initiated after the 90-minute period described above. Therefore, this study provides only two data points without the effects of infusion. However, the full dataset has been successfully modeled by Bert et al. 2000. We use the pre-infusion model results in our comparison.

The model of Bert et al. 2000 is a four-compartment model which includes circulation, red blood cells, interstitial fluid, and interstitial cells. Similar to the CSM, the model calculates mass flows of plasma and proteins between the compartments and, in addition, tracks the redistribution of small ions (Na^+, K^+, Cl^-) and glucose. Bert et al. compared this model to the full data of Tølløfsrud et al. starting with hemorrhage and continuing for three hours after infusion. As a result, their model output includes the effects of hemorrhage and transcapillary refill on plasma volume for the 90 minutes prior to infusion. Because the Bert et al. model fits well with the full dataset including infusion, we are confident in using the model results prior to infusion for comparison with the CSM.

2.3.2. CSM Results

The results of the CSM simulations are provided in Figure 2. The data points of Tølløfsrud et al. are shown as black points with error bars, and the model of Bert et al. 2000 is the dashed blue line. These data were given in the original papers as loss in blood volume (mL). To compare with our data, we converted these values to a plasma volume using a CSM baseline (time = 0) plasma volume of 3200 mL, and scaled blood loss by 55% to get plasma loss. CSM results (red line) show good agreement with both the Bert et al. model and the data. The green dashed line shows results including fluid resuscitation for comparison.

While the modification of the CSM shows good agreement with the comprehensive model of Bert et al. for hemorrhage, more data is required to fully validate the model. The number of hypovolemic studies on humans is limited, but additional data exists on infusion in normovolemic patients and would serve as a useful complement to this study. Future validation work may involve development of animal model parameters in order to validate the modeling approach with experimental animal data.

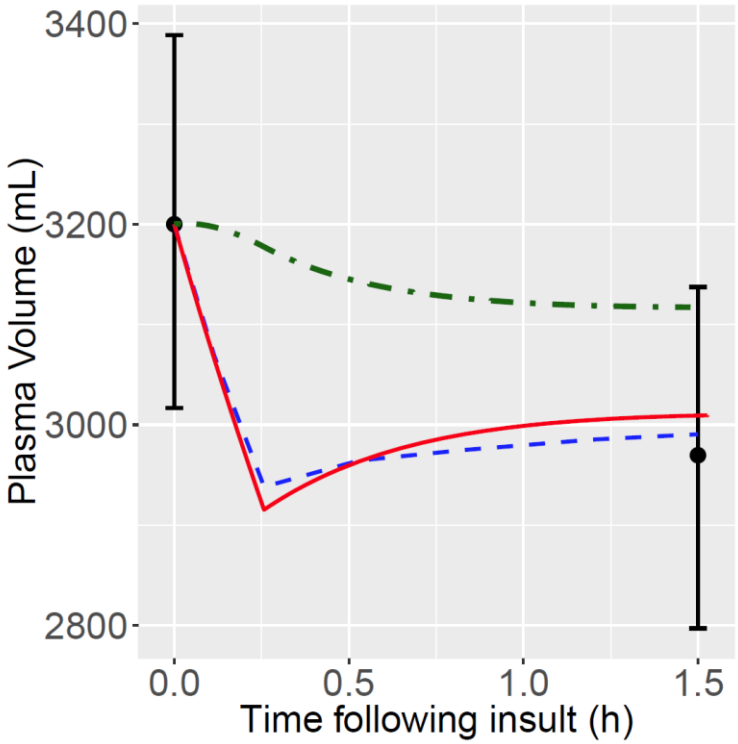

Figure 2. Plasma volume as a function of time for 10% hemorrhage of 15-minute duration

Section 3.

Hematopoiesis After Hemorrhage

3.1 Background

States of decreased and increased blood cell concentrations have been associated with increased mortality risk (Mirsaeidi et al. 2010). Radiation and burn injury lead to significant alterations in hematopoiesis; blood loss due to hemorrhage also impacts hematopoietic dynamics. Mechanistic models of progenitor and blood cell kinetics have been used to simulate how radiation and thermal injury lead to alterations in hematopoiesis (Wentz et al. 2014, 2015). These models provide a valuable starting point for examining the impact of hemorrhage on hematopoietic risk. The intent of these models is to predict synergistic effects of hematopoietic dynamics when simultaneously exposed to multiple insults.

3.1.1. General Hematopoiesis

Hematopoiesis is the process by which mature blood cells are generated from hematopoietic stem cells (HSC) located in the bone marrow. We model hematopoiesis of platelets (thrombocytes), granulocytes (neutrophils), and lymphocytes, due to their importance in recovery from radiation, burn, and hemorrhage. These cells play essential roles in immune response and tissue repair. Perturbations to equilibrium concentrations of these cells can have detrimental effects. Radiation doses above about 1 Gy have a significant impact on blood cells by directly killing early progenitor cells and perturbing hematopoiesis through mediator-related processes.

It is important to understand the responses of each of these cell types to combined injury and how it affects their functionality. Platelets help stop bleeding in the event of hemorrhage; this process is inhibited when radiation and burn reduce the number of progenitor and functioning platelets required for clotting. Combined injury can also have synergistic effects on white blood cells (WBCs). For instance, burn increases permeability, resulting in bacterial translocation, while burn, radiation and hemorrhage result in cell death/loss of functioning WBCs needed to fight infection.

Mathematical models can be used to understand the impacts of radiation on blood cell dynamics, depletion of different cell lines, and the timeframe of recovery. A number of existing models (Gräßle 2000; Akushevich 2011) describe the kinetics of different blood cell lineages. Russian mathematical biologist, Olga A. Smirnova, previously published models of thrombopoiesis, granulopoiesis, and lymphopoieses which describe the effect of radiation on blood cell dynamics (Smirnova 2010, 2012). These models were updated, fully documented, and validated in Wentz et al. 2014. Expansion of these models allowed for the added response to burn in Wentz et al. 2015. In the current study, we add the effects of hemorrhage to each of these models, providing the capability to predict outcomes from combined radiation, burn and hemorrhage insults.

Each model discussed in this section is based on the same general structure of hematopoiesis. The diagram in Figure 3 illustrates these dynamics, which originate in the bone marrow with dividing progenitor cells. These cells give way to non-dividing progenitor cells, which eventually mature and enter the bloodstream. Radiation causes cells to enter damaged states before they undergo an early death. Depending on the hematopoietic cell line, each cell type has a different

level of radiosensitivity. Similarly, burn affects different cellular processes (proliferation rates, maturation rates, etc.) depending on the cell type. The general hematopoiesis diagram does not incorporate burn and hemorrhage effects, which vary by hematopoietic cell line. For a more detailed description of the model structure, including specific differences between the three models, see Wentz et al. 2014, 2015. These reports also provide details on procedures and data used for parameter selection and model validation.

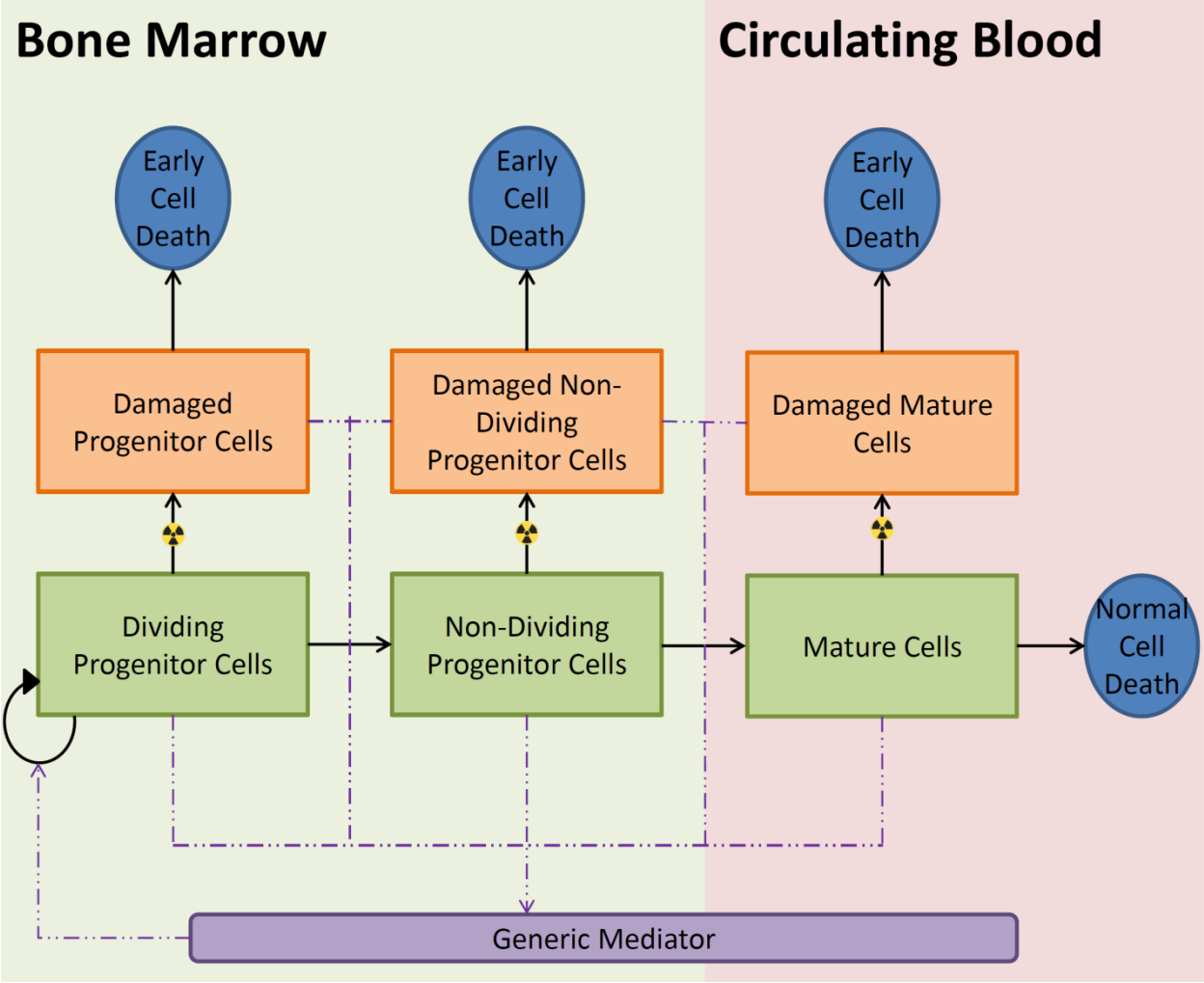

Figure 3. Diagram of the generic hematopoietic model structure

3.1.2. Method for Integrating Hemorrhage

The impact of hemorrhage was incorporated into the models of each hematopoietic cell line (thrombocytes, granulocytes and lymphocytes) to simulate hematopoietic response and recovery to blood loss. Mouse and human parameter sets have been developed for each of these models, taking advantage of the data sets available for both species.

Acute hemorrhage is modeled the same way in each blood cell line. We assume that the blood loss and the fluid refill occur on fast time scales. With these assumptions, we apply an

instantaneous removal of cells from the concentration in circulation x_c, equal to the total percentage of blood lost (PBL) from hemorrhage:

$$x_c(0) = \bar{x}_c\left(1 - \frac{PBL}{100}\right) \quad (2)$$

where $x_c(0)$ is the concentration of cells in circulation at the time of hemorrhage and $\bar{x}_c$ is the normal concentration of cells in circulation. In response to cell loss, circulating granulocytes experience a rapid influx of cells from a subcompartment of marginated cells adhered to the blood vessel walls. We include this process, called 'demargination,' in the granulocyte model. Diagrams of each model with the updated hemorrhage effects are provided in Figure 4, Figure 7, and Figure 10.

3.2 Thrombopoiesis Model

Thrombopoiesis is the process of platelet formation. Platelets are responsible for the coagulation of blood and are a source of growth factors, which regulate cell growth and division. Platelet generation is initiated by self-renewing hematopoietic stem cells (HSCs) in the bone marrow. These stem cells differentiate, and, through a series of mitotic divisions, produce megakaryocytes (MKs), the precursors of platelets. As MKs mature, their ploidy increases, through a series of endomitoses. Once matured, MKs produce platelets, which enter the bloodstream.

The first compartment of the thrombopoiesis model (Figure 4) represents mitotic precursors in the bone marrow. This compartment represents various cell types ranging from HSCs to megakaryoblasts. MKs are divided into immature and mature compartments in the bone marrow. Each MK produces thousands of platelets, resulting in amplification of platelet generation. Following radiation exposure in humans, there is a delay before the peripheral platelet counts begin to decline (Bond et al. 1965). This delay is due, in part, to the maturation time of early progenitors affected by radiation. Sub-compartments were added to the immature and mature MK compartments in order to simulate this delayed effect. The fourth and final compartment represents platelets in circulation. The platelet compartment is also divided into sub-compartments to generate more biologically realistic transit time distributions (Murphy et al. 1971).

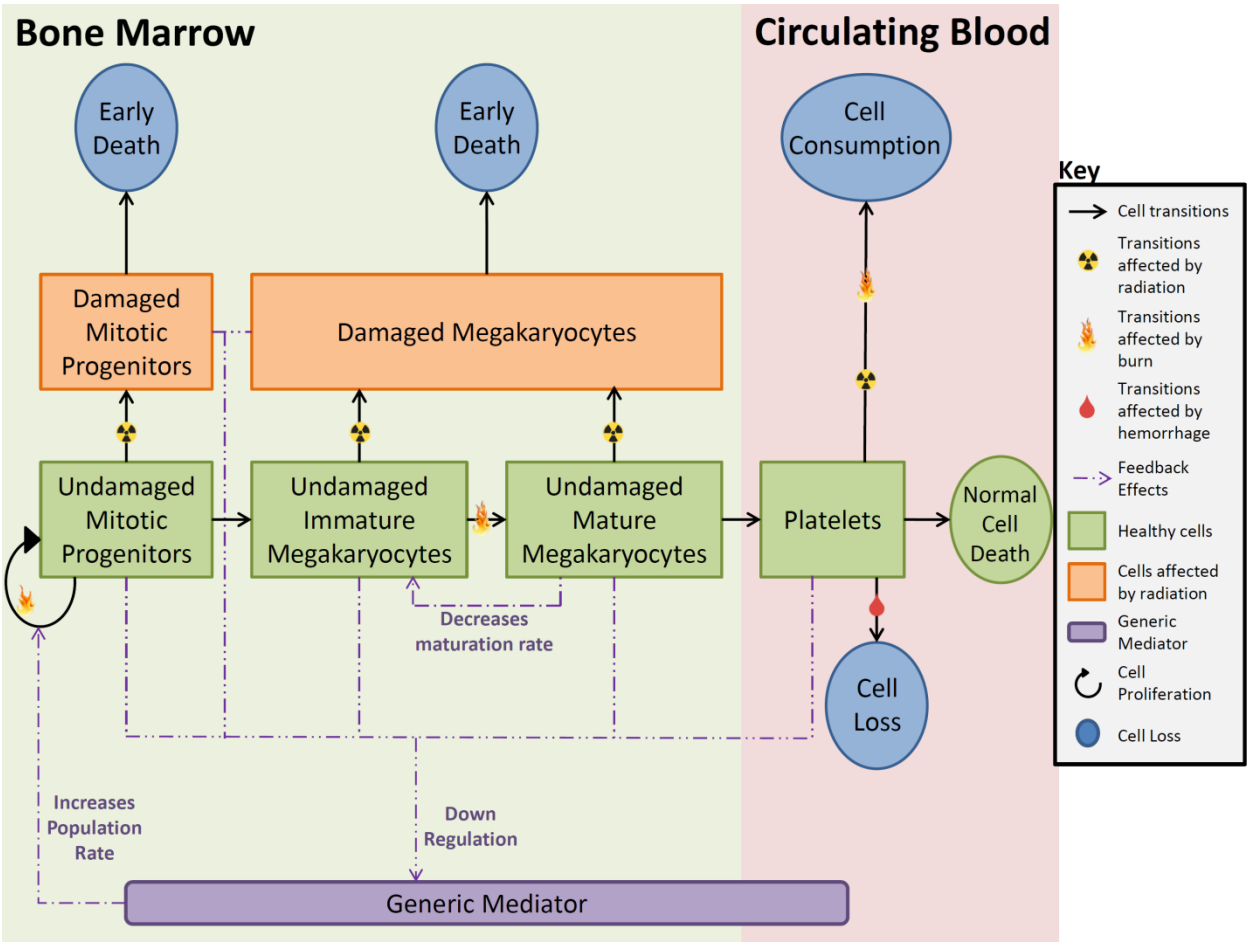

Figure 4. Diagram of the thrombopoiesis model structure

When simulating hemorrhagic effects with the hematopoietic models, we found it appropriate to compare the ability of each model to reproduce data reported from blood donations. There are studies which report platelet recovery following thrombocytapheresis (TP), a process in which blood is drawn from a donor, platelets are extracted from whole blood products, and the remaining portions of blood are returned to the donor. Table A-1 summarizes the TP data collected and simulated with the thrombopoiesis model. Plateletpheresis studies were simulated by setting the initial platelet concentration in the model to the platelet concentration reported directly after donation. Within Figure 5 and Figure 6, which provide comparisons of model simulations to two of these experiments, data points are provided in black (± standard deviations), simulations are represented with a red solid line, and a dashed black horizontal line represents the average baseline concentration. In Lasky 1981 (Figure 5), 33 individuals provided platelet samples for up to 20 days following TP, and platelet data from two donors were reported up to 20 days after platelet donation in Sullivan 1977 (Figure 6). The remaining TP simulations are provided in Appendix B-1 (Figure B-1 to Figure B-4).

Ideally, we would like to compare the model to platelet data after whole blood donation, which is more representative of the effects of hemorrhage than plateletpheresis. Furthermore, it would be ideal to have hemorrhage data where the PBL is larger than the normal blood donation amount which is around 8% (Starr and Starr 2013). We have not found data of this nature, but we expect thrombocytapheresis to result in effects similar to blood loss by causing a reduction in circulating platelet cells. The model captures the dynamics of platelet recovery, as well as an overshoot of platelet counts above the baseline. The accuracy of this model is important because it has been shown that platelet count is associated with risk of mortality (Akca et al. 2002).

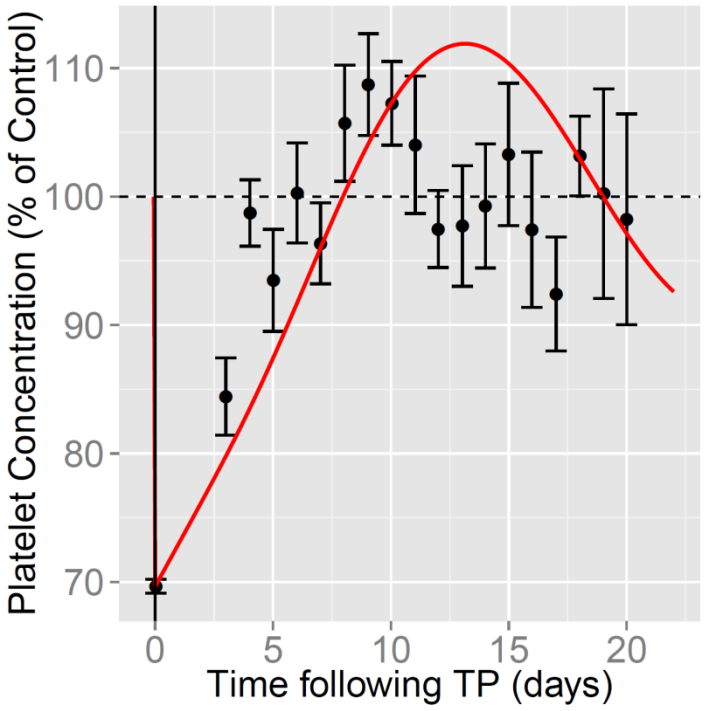

Figure 5. Simulation of plateletpheresis (Lasky et al. 1981) with the thrombopoiesis model

As discussed earlier, a main objective of the hematopoietic models is to accurately predict combined injury effects. At this point, we have developed and validated the thrombopoiesis model against radiation, burn, and hemorrhage insults individually. We intend to appropriate data of combined injuries in the future and to assess the model's current ability to predict the effects from multiple acute injuries.

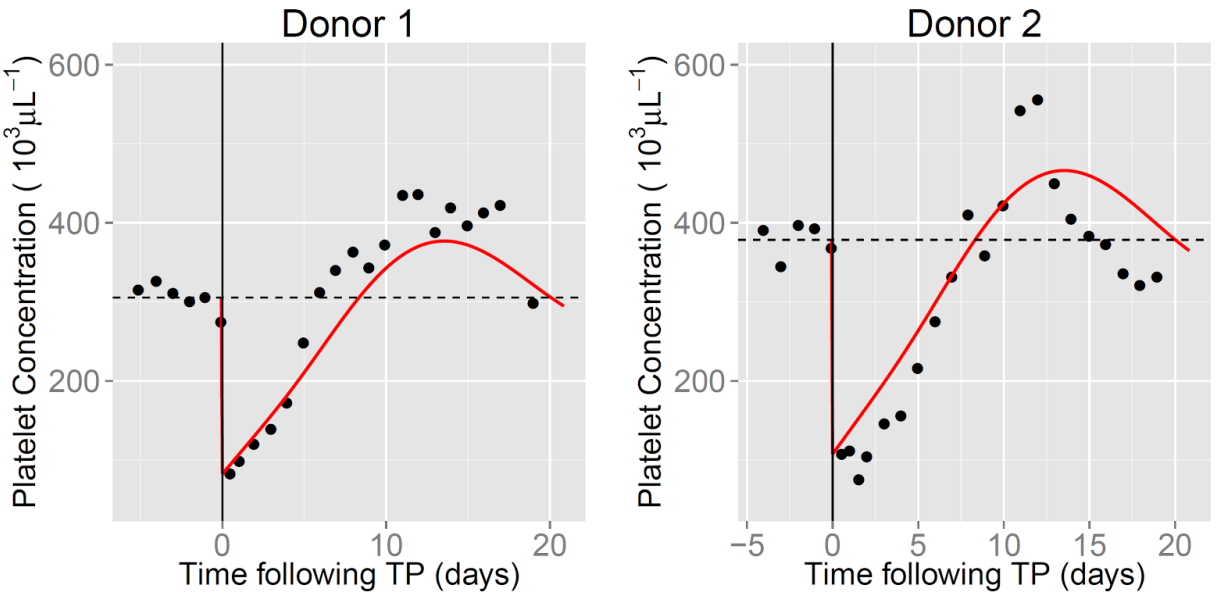

Figure 6. Simulation of plateletpheresis (Sullivan et al. 1977) with the thrombopoiesis model

3.3 Granulopoiesis Model

Granulopoiesis is the process by which mature granulocytes are generated from pluripotent HSCs. Granulocytes are a type of leukocyte that can be subdivided into neutrophils, eosinophils, and basophils. Neutrophils account for the majority of granulocytes and are involved in phagocytosis, the process which engulfs a solid particle such as bacteria. Neutrophils are also responsible for generating neutrophil extracellular traps (NETs), which help control microbial infection. Granulocytes are important for quickly responding to infection, and granulocytopenia, an abnormally low granulocyte concentration, can result in the body's inability to fight infection.

The granulopoiesis model (Figure 7) has four compartments: mitotic precursors in the bone marrow, post-mitotic precursors in the bone marrow, granulocytes in circulation, and granulocytes in tissues. All cells in the granulopoietic lineage are radiosensitive. The mitotic cells in the bone marrow are the most radiosensitive and become either damaged or weakly damaged. The cells in the other three compartments are less radiosensitive than mitotic cells and enter a single damaged state following radiation exposure. The weakly damaged cell compartment is used to model the late transient increase in granulocyte counts observed following radiation exposure (Bond et al. 1965).

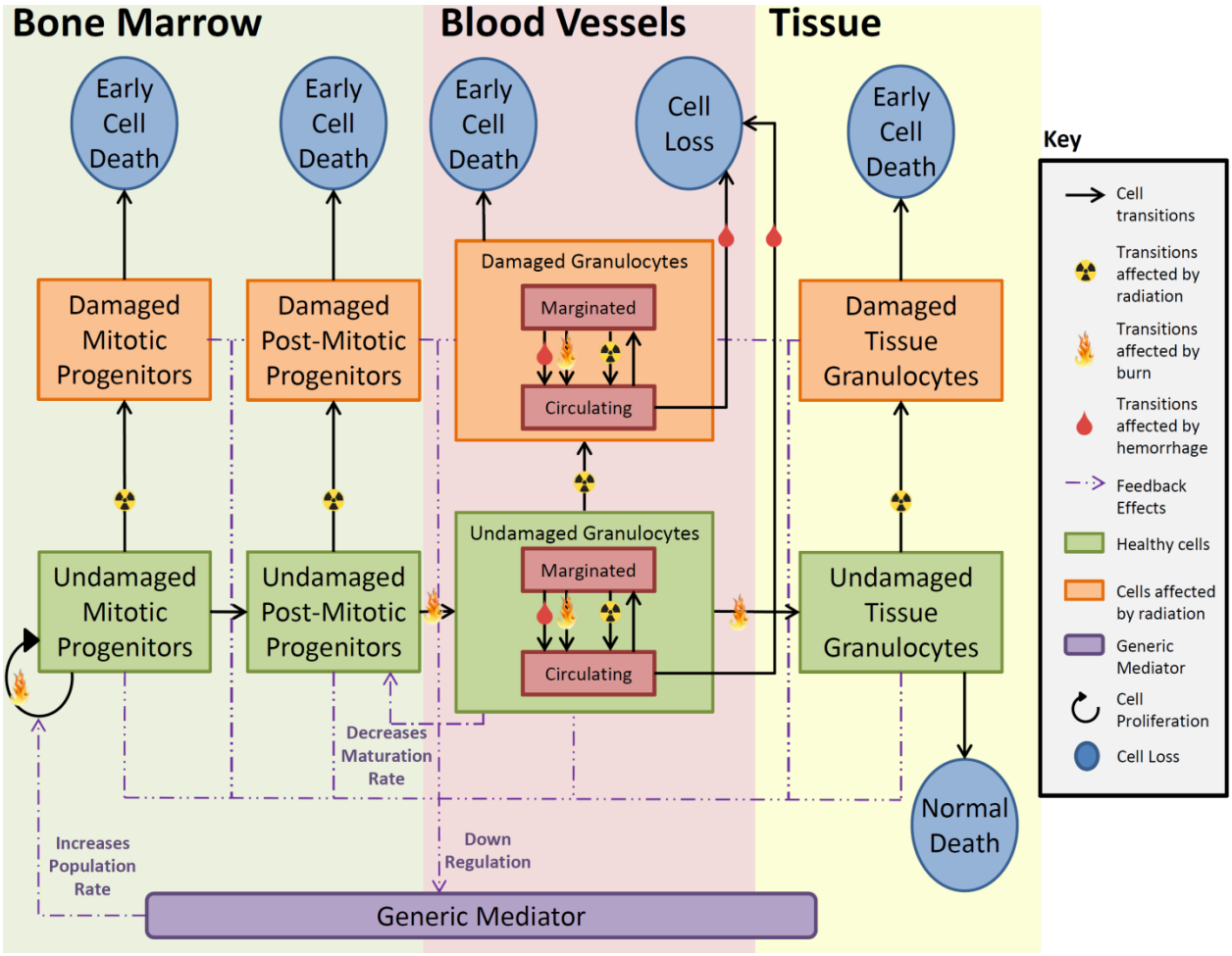

Figure 7. Diagram of the granulopoiesis model structure

3.3.1. Granulocyte Demargination

It has been reported that granulocytes adhere to the lining of blood vessels, removing themselves in response to insults and increasing the concentration of granulocytes in circulation in a process called demargination (Summers et al. 2010). Previously (Wentz et al. 2015), demargination was included in the model, but only in response to burn. In the current study, we include granulocyte demargination in response to radiation and hemorrhage with the same function used to describe burn-induced demargination. The function $r(t)$ determines the percentage of granulocytes in circulation, and has the following form:

$$r(t) = \bar{r}(1 + f(I)e^{-at})$$
$$f(I) = b\frac{(A+1)I^k}{A + I^k} \quad (3)$$

In Equation (3), $\bar{r}$ is the normal percentage of demarginated cells (approximately 0.25 for mice (Johnson et al. 1995) and 0.5 for humans (Summers et al. 2010)), I is the magnitude of insult (radiation dose, % TBSA burned, or PBL from hemorrhage), a is the demargination relaxation rate which determines how quickly the system returns to normal ($r \rightarrow \bar{r}$) and b, A, and k determine the amplitude of the demargination response.

Parameters a, b, A, and k are insult-specific and have previously been determined for the murine and human models in the context of burn (Wentz et al. 2015). We will use subscripts 'b', 'r', and 'h' to distinguish between burn, radiation, and hemorrhage insults, respectively and 'm' and 'h' to distinguish between murine and human models, respectively (for example, $a_{h,m}$ is the demargination relaxation rate, a, for the murine model in the context of hemorrhage). In this study, we determined human and murine parameter values for radiation-induced demargination as well as murine hemorrhage-induced demargination parameters. Due to a lack of data, we extrapolate human hemorrhage-induced demargination parameters from the murine model.

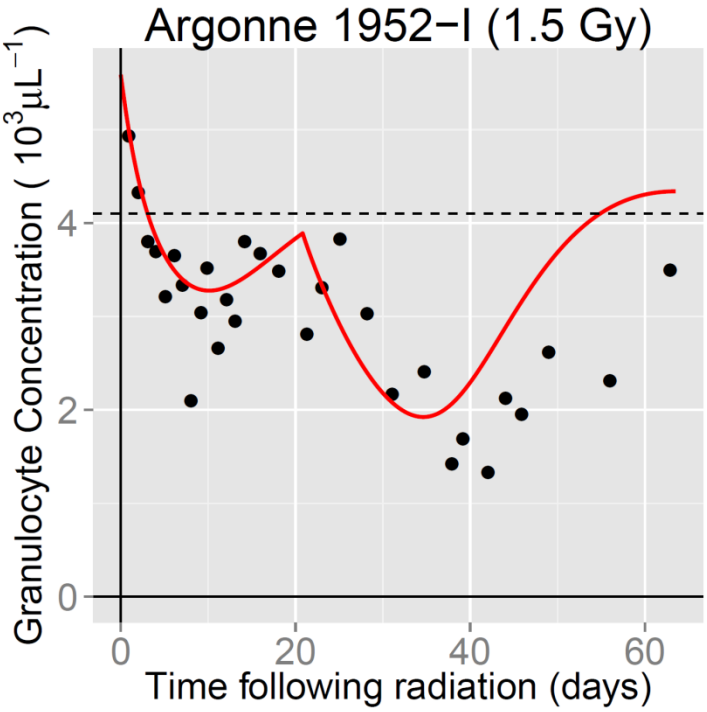

Figure 8. Radiation-induced demargination of granulocytes

3.3.2. Granulocyte Cell Kinetics following Radiation

In Wentz et al. 2014, the human and murine granulocyte models were parameterized using a set of radiation accident data and experimental data. Using the same data, we have optimized human and murine values for a_r and b_r, A_r, and k_r (details provided in Appendix A). Figure 8 provides an example of the human granulocyte model simulating a 1952 radiation incident at the Argonne National Laboratory (Bond et al. 1965). The updated model does an improved job of capturing the acute increase of circulating granulocytes following a radiation insult compared to the model in Wentz et al. 2014 which does not include demargination. Simulations of the remaining studies for human and murine data are provided in Figure B-5 - Figure B-17.

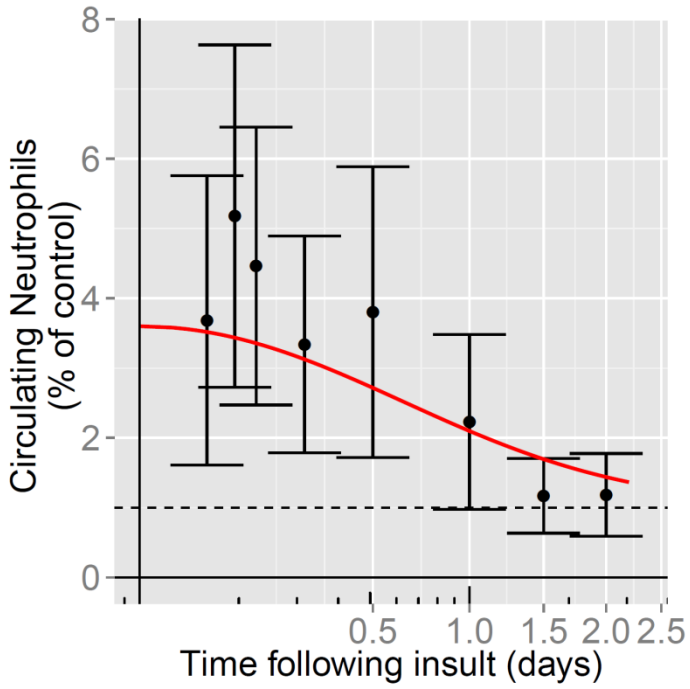

Figure 9. Murine neutrophil data (Gaylor et al. 1969) following hemorrhage

3.3.3. Granulocyte Cell Kinetics following Hemorrhage

There are a limited number of studies reporting granulocyte concentration following hemorrhage. In Gaylor et al. 1969, neutrophils of mice were reported after a 40% blood loss for up to 4 days following hemorrhage. We used the experimental data from this study to parameterize a_h, b_h, k_h and A_h in the murine model (details provided in Appendix A, parameters in Table A-3). Simulating this experiment in Figure 9, we see the model is able to capture the increased concentration of granulocytes in circulation as well as the delayed return to a normal ratio of marginated to demarginated cells. We have been unable to find human granulocyte data following hemorrhage. In order to parameterize the human hemorrhage-induced demargination parameters, we have utilized the murine model. We compared the differences between human and murine demargination in response to radiation, and used this relationship to determine $a_{h,h}$, $b_{h,h}$, $A_{h,h}$ and $k_{h,h}$ from $a_{h,m}$, $b_{h,m}$, $A_{h,m}$ and $k_{h,m}$ (details in Appendix A, parameters in Table A-3). Until we have time-dependent human granulocyte data following granulocyte loss, we will be unable to validate our human model of granulocyte demargination response.

3.4 Lymphopoiesis Model

The lymphopoiesis model (Figure 10) consists of three compartments: mitotic precursors in the bone marrow, post-mitotic precursors in the bone marrow or thymus, and lymphocytes in circulation. All cells in the lymphopoiesis model are considered radiosensitive and, once damaged, decay at a specific rate. Radiation and burn effects have been captured with the lymphocyte model (Wentz et al. 2014, 2015) and hemorrhage effects are assumed to reduce the circulating cells, as we have done with the other hematopoietic models.

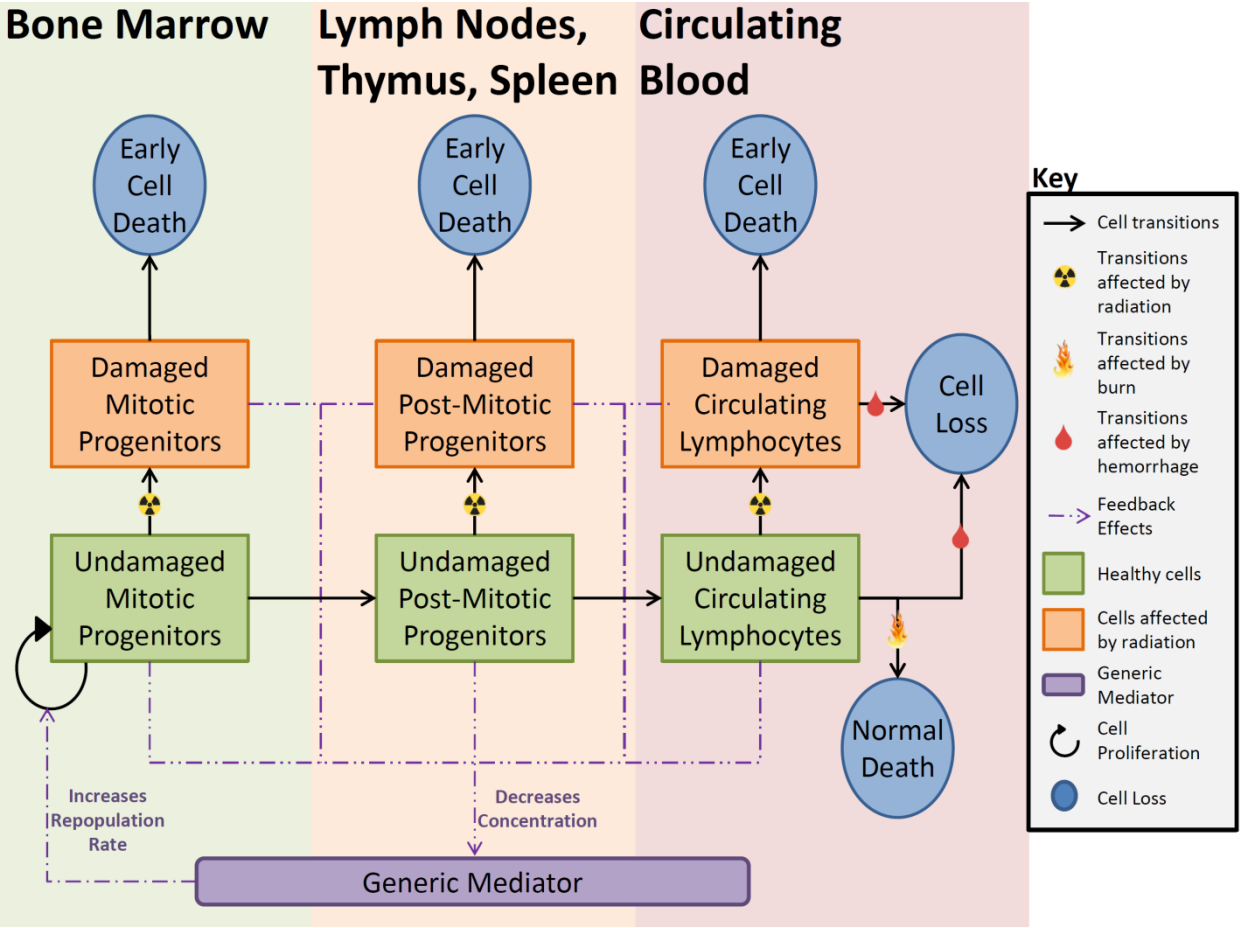

Figure 10. Diagram of the lymphopoiesis model structure

When simulating a human experiment of lymphocyte counts following blood donation (Smetana et al. 1983), we found that our model is unable to capture these unexpected dynamics (Figure 11). In Smetana et al. 1983, lymphocyte counts of 27 blood donors are measured up to 55 days following blood donation. There is a consistently large, abrupt rise in lymphocyte concentrations between all patients within the first day following blood loss. This lymphocytosis is dampened over the course of the study until the lymphocyte counts return to normal. A similar result was reported in swine (Hawksworth et al. 2012) where a rise in lymphocyte counts can be seen during a reperfusion stage following a grade III liver injury with uncontrolled hemorrhage (Figure 12). There is a slight rise in lymphocytes one day following hemorrhage, but this is much smaller than the rise reported with the human data.

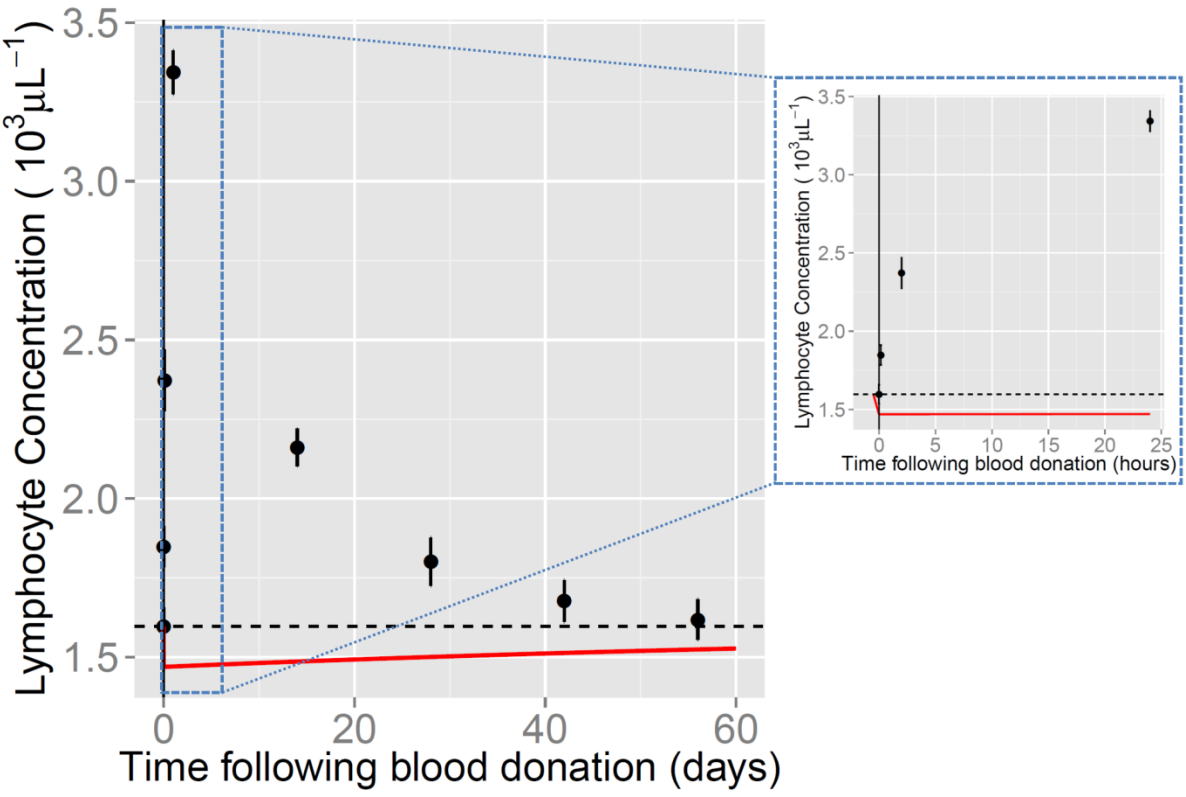

Figure 11. Lymphocytes following hemorrhage

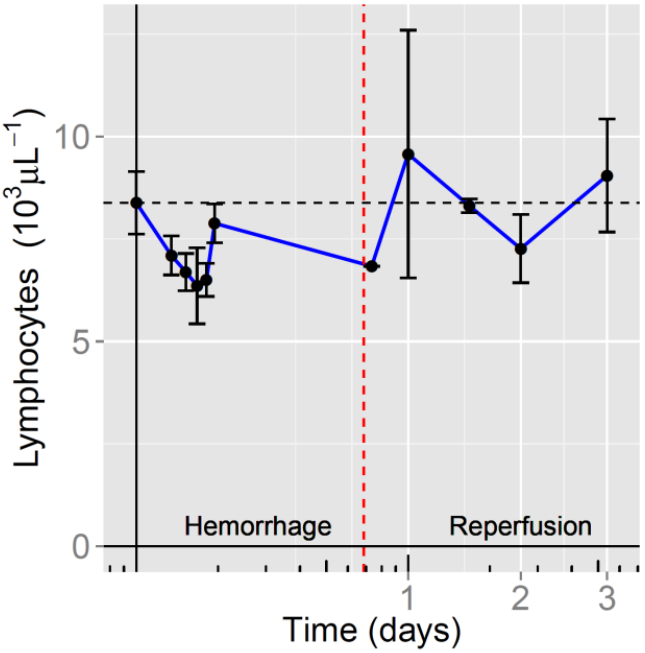

Figure 12. Experimental data of swine lymphocyte response to hemorrhage

The lymphocyte hemorrhage model only assumes recovery after loss, so it is unable to capture any upsurge. We are not certain what causes this jump in lymphocytes, but we hypothesize that it is an insult-driven response of the system delivering function-specific lymphocytes to counter the irregularity. The response appears to be very strong, and the return to a baseline lymphocyte level follows an exponential decay with a short half-life. This response and quick recovery follows the description of effector cell response, where the majority of effector T cells have short lives (Tough and Sprent 1995). It is possible a reservoir of effector cells is being dumped into circulation and this trend is representative of that particular subset of lymphocytes. Further research is necessary to resolve this question.

3.5 Modeling Combined Hemorrhage and Radiation

There are very few studies of hematopoietic response to combined injury, most of which are non-human. In order to validate our models, which now include response to radiation, burn and hemorrhage, we analyzed a study reporting the hematopoietic kinetics of mice following combined injury. Kiang et al. 2015 is the only study we are aware of that provides neutrophil, lymphocyte and platelet counts after combined radiation and hemorrhage. Platelet concentration is reported seven days after insult and neutrophil and lymphocyte concentrations are reported two days following insult. The injuries consist of a 20% blood loss hemorrhage, an 8.75 Gy dose of radiation or a combination of these injuries, where hemorrhage was administered one hour after irradiation.

We simulated the experiment using the murine model, and the results are provided in Figure 13. In each subfigure, the model simulation is shown in red compared to the data point two or seven days post-insult. Baseline platelet or white blood cell concentrations are provided with a horizontal dashed black line. The combined injury was simulated by solving the model with radiation for one hour before applying the appropriate reduction in circulating cells. For the granulocyte model, we assumed the demargination was dominated by the maximum demargination response. That is, we set:

$$r(t) = \max_{t \geq 0}(r_h(t), r_r(t)) , \tag{4}$$

where r_h and r_r represent the ratio of circulating cells in the blood vessels (demarginated) from hemorrhage and radiation insults, respectively.

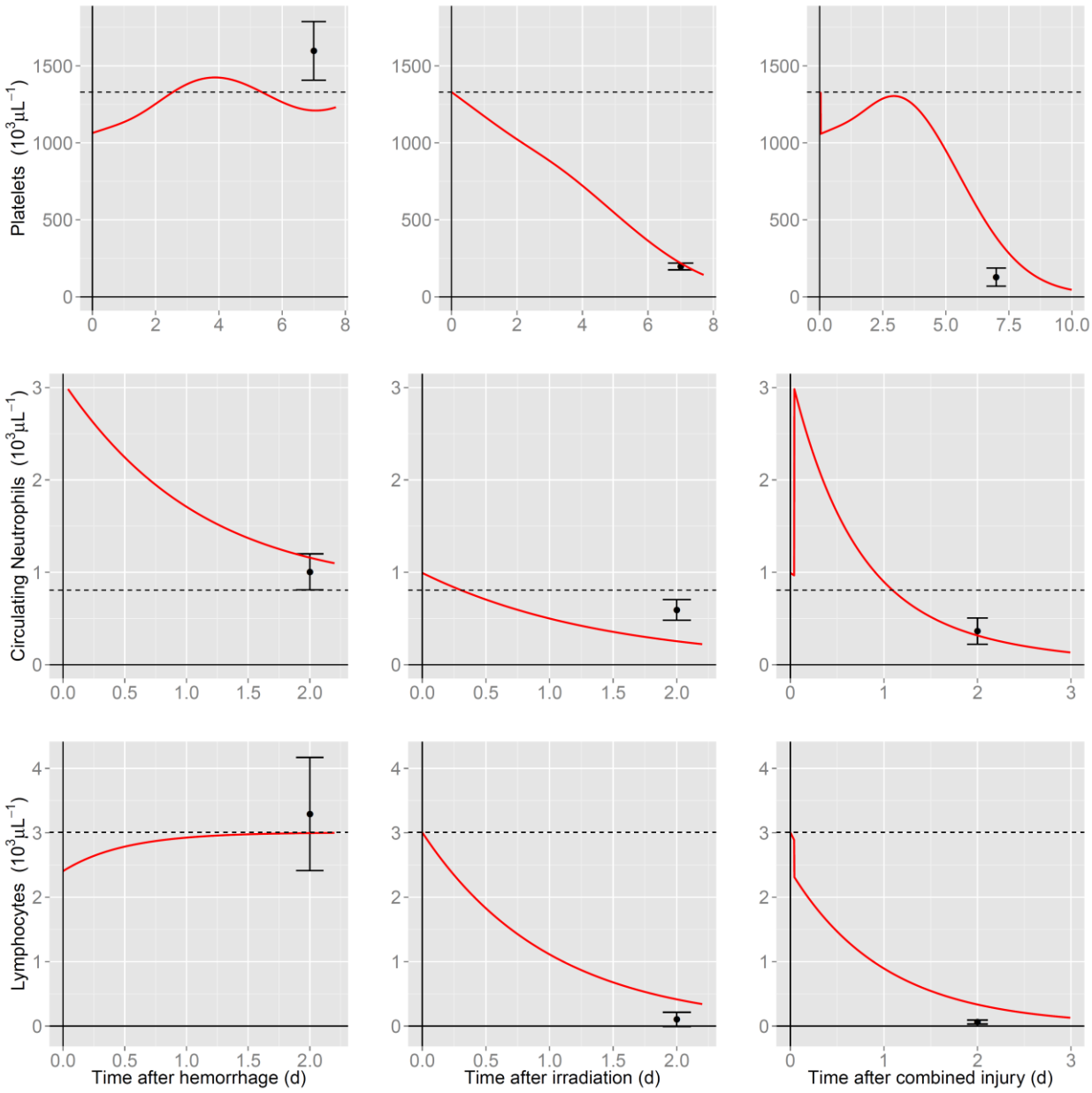

Figure 13. Murine hematopoietic response to combined radiation and burn injuries

According to the data in Figure 13, Hemorrhage alone has a small impact on platelet, neutrophil and lymphocyte counts. In fact, seven days following hemorrhage, there is a reported rise in platelets, and two days after hemorrhage there is a small increase in neutrophils and lymphocytes from baseline values. The model captures these particular measurements, but the sparse nature of the data makes it impossible to evaluate the validity of the model before or after these points. Similarly, the model is generally accurate when simulating the radiation experiment for the three cell types, slightly underestimating the number of neutrophils and slightly overestimating the number of granulocytes two days post-insult. The model does a surprisingly good job of capturing the effects of the combined injury. Although the model overestimates the number of platelets and lymphocytes following the insults, the differences between the simulation and the data are small.

3.6 Discussion

The human hematopoietic models capture the basic trends in the dynamics of the different hematopoietic cell types in response to radiation, burn and hemorrhage injuries where data is available. Including radiation and hemorrhage-induced demargination in the granulocyte model has further improved the accuracy of this model. We have found combined injury data for mice, which has helped validate the murine model. The human and murine models have been built on the same principles, and the human model relies on the murine model for hemorrhage-induced granulocyte demargination. More human data would be useful for future model calibration and validation.

Section 4.

Summary

4.1 Models to date

The CSM and hematopoietic models have been updated to include the impact of hemorrhage on fluid dynamics and hematopoietic cell kinetics, respectively. While a number of more detailed mechanistic attributes may be warranted in future studies, the current models provide an estimate of the additive and/or synergistic impacts of combined injury on the key mechanisms associated with mortality for use in casualty estimation. Further improvements and validations of the models may be accomplished by working with experimentalists to gain more data for use in each of our models.

4.2 Future work

The following sections provide an overview of future work in regards to this research. The subsections discuss model improvements, additional mechanistic models of combined injury and predicting the risk of outcomes from model outputs.

4.2.1. Model Improvements and Additional Validation

We will continue to update the human and murine hematopoietic models as data becomes available. To date, we have not found any relevant human granulocyte data following blood loss, and only one study reporting lymphocytes after hemorrhage (Smetana et al. 1983). With more in-depth studies, verification of our lymphocyte relocation hypothesis would also be possible, and we could include acute response of reservoir lymphocytes, similar to our approach with granulocyte demargination. If available, we can use a non-human primate (NHP) model. In theory, this should make extrapolations more accurate.

For hemorrhage, some additional human studies exist for blood loss of less than 10% total blood volume. These could be used for additional model validation, if required. For times longer than approximately two hours after hemorrhage, all studies include fluid resuscitation. A fluid resuscitation model would need to be added to the CSM before these studies could be used for validation at times longer than two hours.

4.2.2. Other Mechanistic Models

In addition to hemodynamics and hematopoiesis, we are modeling other physiological systems to complete the picture of combined injury. For instance, a model of the small intestinal cell kinetics after radiation and burn is currently in development. Radiation and burn can damage the gut, which can increase gut permeability and restrict nutrient absorption. Hemorrhage impacts the gut in a manner similar to burn, where hypovolemia and ischemia can result. Therefore, the impact of hemorrhage will also be added to the small intestine model in the future. Hemorrhage results in damage to cells through various protein signaling pathways. Kiang et al. showed that

an activated iNOS (inducible nitric oxide synthase) pathway causes an activation of caspase-3, leading to an increase of apoptosis of cells in the small intestine (Kiang et al. 2011). We have developed a mathematical model of the small intestine cell kinetics which responds to radiation and burn injuries, but does not capture the response to hemorrhage. In the future, we will coordinate with experimentalists to collect quantifiable histological data in order to incorporate this response in our small intestine cell kinetic model.

4.2.3. Mapping Model Outputs to Predicting Risk of Outcomes

Finally, each of our mechanistic models provides clinically relevant outputs. These outputs will be further related to risk of mortality, whether through shock or sepsis. We can leverage this risk mapping to allow for a more reliable prediction of time-to-mortality based on the response of the clinical parameters with time.

Section 5.

References

Akca S, Haji-Michael P, de Mendonça A, Suter P, Levi M, Vincent J. Time course of platelet counts in critically ill patients. Critical Care Medicine 30(4):753-756; 2002.

Akushevich IV, Veremeyva GA, Dimov GP, Ukraintseva SV, Arbeev KG, Akleyev AV, Yashin AI. Modeling hematopoietic system response caused by chronic exposure to ionizing radiation. Radiation and Environmental Biophysics 50(2):299-311; 2011.

Ampratwum RT, Bowen BD, Lund T, Reed RK, Bert JL. A model of fluid resuscitation following burn injury: formulation and parameter estimation. Computer Methods and Programs in Biomedicine 47(1):1-19; 1995.

Andrews GA, Sitterson BW, Kretchmar AL, Brucer M. Criticality accident at the Y-12 plant. Diagnosis and Treatment of Acute Radiation Injury 27-48; 1961.

Ardia D, Mullen KM, Ulrich J, Peterson BG. DEoptim: An R Package for Global Optimization by Differential Evolution. R Project; 2015.

Barnea O, Sheffer N. A computer model for analysis of fluid resuscitation. Computers in Biology and Medicine 23(6):443-454; 1993.

Bert JL, Gyenge CC, Bowen BD, Reed RK, Lund T. A model of fluid and solute exchange in the human: validation and implications. Acta Physiologica Scandinavica 170(3):201-209; 2000.

Bolton PM, Kirov SM, Donald KJ. The effects of major and minor trauma on lymphocyte kinetics in mice. The Australian Journal of Experimental Biology and Medical Science 57(5):479-492; 1979.

Bond VP, Fliedner TM, Archambeau JO. Mammalian radiation lethality: A disturbance in cellular kinetics. New York: Academic Press; 1965: 78-83.

Brecher G, Endicott KM, Gump H, Brawner HP. Effects of X-ray on lymphoid and hemopoietic tissues of albino mice. Blood 3(11):1259-1274; 1948.

Carlson DE, Kligman MD, Gann DS. Impairment of blood volume restitution after large hemorrhage: a mathematical model. The American Journal of Physiology 270(5):R1163-R1177; 1996.

Cope O, Litwin SB. Contribution of the lymphatic system to the replenishment of plasma volume following hemorrhage. Annals of Surgery 156:655-667; 1962.

Davis TA, Landauer MR, Mog SR, Barshishat-Kupper M, Zins SR, Amare MF, Day RM. Timing of captopril administration determines radiation protection or radiation sensitization in a murine model of total body irradiation. Experimental Hematology 38(4):270-281; 2010.

Dettke M, Hlousek M, Kurz M, Leitner G, Rosskopf K, Stiegler G, Stohlawetz P, Worel N, Höcker P, Panzer S. Increase in endogenous thrombopoietin in healthy donors after automated plateletpheresis. Transfusion 38(5):449-453; 1998.

Doherty TJ. A mathematical model for the study of hemorrhagic shock and fluid resuscitation: The systemic and pulmonary vasculature. Tech. rep. 479. Division of Military Trauma Research; 1993.

Drucker, WR, Chadwick, CDJ, Gann DS. Transcapillary refill in hemorrhage and shock. Archives of Surgery 116(10):1344-1353;1981.

Fontana S, Rados L, Schmid P, Leibundgut EO, Taleghani BM. Recruitment of platelets, white blood cells, and hematopoietic progenitor cells during high-yield plateletpheresis. Transfusion 51(9):2034-2043; 2011.

Fülöp A, Turóczi Z, Garbaisz D, Harsányi L, Szijártó. Experimental models of hemorrhagic shock: A review. European Surgical Research 50:57-70; 2013.

Furth R, Sluiter W. Distribution of blood monocytes between a marginating and a circulating pool. The Journal of Experimental Medicine 163(2):474-479; 1986.

Gann DS, Carlson DE, Byrnes GJ, Pirkle JC, Allen-Rowlands CF. Impaired restitution of blood volume after large hemorrhage. The Journal of Trauma 21(8):598-603; 1981.

Ghosh SP, Kulkarni S, Perkins MW, Hieber K, Pessu RL, Gambles K, Maniar M, Kao TC, Seed TM, Kumar KS. Amelioration of radiation-induced hematopoietic and gastrointestinal damage by Ex-RAD(R) in mice. Journal of Radiation Research 53(4):526-536; 2012.

Gräßle DH. Simulation of radiation effects using biomathematical models of the megakaryocytic cell renewal system. Universität Ulm, Medizinische Fakultät; 2000.

Gyenge CC, Bowen BD, Reed RK, Bert JL. Preliminary model of fluid and solute distribution and transport during hemorrhage. Annals of Biomedical Engineering 31(7):823-839; 2003.

Hawksworth JS, Graybill C, Brown TS, Gillern SM, Wallace SM, Davis TA, Elster EA, Tadaki DK. Lymphocyte depletion in experimental hemorrhagic shock in swine. Journal of Inflammation 9(1):1; 2012.

Hempelmann LH, Lisco H, Hoffman JG. The acute radiation syndrome: a study of nine cases and a review of the problem. Annals of Internal Medicine 36(2):279-510; 1952.

Hirama T, Tanosaki S, Kandatsu S, Kuroiwa N, Kamada T, Tsuji H, Yamada S, Katoh H, Yamamoto N, Suzuki G, Akashi M. Initial medical management of patients severely irradiated in the Tokai-mura criticality accident. British Journal of Radiology 76(904): 246-253; 2003.

Howland J, Ingram M, Mermagen H, Hansen C. "The Lockport incident: Accidental partial body exposure of humans to large doses of X-irradiation," *Diagnosis and Treatment of Acute Radiation Injury: Proceedings of a Scientific Meeting Jointly Sponsored by the IAEA and the WHO, Geneva*, 17-21 Oct 1960. Columbia University Press, New York, 11-26.

Johnson RC, Mayadas TN, Frenette PS, Mebius RE, Subramaniam M, Lacasce A, Hynes RO, Wagner DD. Blood cell dynamics in P-selectin-deficient mice. Blood 86(3):1106-1114; 1995.

Jammet H, Mathé G, Pendic B, Duplan JF, Maupin B, Latarjet R, Kalic D, Schwarzenberg L, Djukic Z, Vigne J. Study of six cases of accidental acute total irradiation. In: Johnson

RC, Mayadas TN, Frenette PS, Mebius RE, Subramaniam M, Lacasce A, Hynes RO, Wagner DD. Blood cell dynamics in P-selectin-deficient mice. Blood 86(3):1106-1114; 1995.

Kemming G, Messick JB, Mueller W, Enders G, Meisner F, Muenzing S, Kisch-Wedel H, Schropp A, Wojtczyk C, Packert K, Messmer K, Thein E. Can we continue research in splenectomized dogs? Mycoplasma haemocanis: old problem – new insight. European Surgical Research 33:198-205; (2004).

Kerr GG, Tankersley WG. External radiation dose estimates for individuals near the 1958 criticality accident at the Oak Ridge Y-12 plant. Tech. rep. ORAUT-OTIB0057. Oak Ridge, TN: Oak Ridge Associated Universities; 2006: 1-21.

Kiang JG, Agravante NG, Smth JT, Bowman PD. 17-DMAG diminishes hemorrhage-induced small intestine injury by elevating Bcl-2 protein and inhibiting iNOS pathway, TNF increase, and caspase-3 activation. Cell and Bioscience 1(1); 2011.

Kiang JG, Smith JT, Anderson MN, Swift JM, Christensen CL, Gupta P, Balakathiresan N, Maheshwari RK. Hemorrhage exacerbates radiation effects on survival, leukocytopenia, thrombopenia, erythropenia, bone marrow cell depletion and hematopoiesis, and inflammation-associated microRNAs expression in the kidney. PLOS One; 2015.

Kulkarni S, Chakraborty K, Kumar KS, Kao TC, Hauer-Jensen M, Ghosh SP. Synergistic radioprotection by gamma-tocotrienol and pentoxifylline: Role of cAMP signaling. ISRN Radiology:1-11; 2013.

Lasky LC, Lin A, Kahn RA, McCullough J. Donor platelet response and product quality assurance in platelet pheresis. Tranfusion 21(3):247-260; 1981.

Latenser BA. Critical care of the burn patient: the first 48 hours. Critical Care Medicine 37(10):2819-2826; 2009.

Mazzoni MC, Borgström P, Arfors KE, Intaglietta M. Dynamic fluid redistribution in hyperosmotic resuscitation of hypovolemic hemorrhage. American Journal of Physiology 255(3):H629-H637; 1988.

Mettler, F A. (2001). “Accidents in industrial radiation facilities”. *Medical Management of Radiation Accidents*. Ed. by I. A. Gusev, A. K. Guskova, and F. A. Mettler. 2nd. CRC Press, Boca Raton, 211-222.

Miller LS, Fletcher GH, Gerstner HB. Radiobiologic observations on cancer patients treated with whole-body X-irradiation. Radiation Research 8(2):150-165; 1958.

Mirsaeidi M, Peyrani P, Aliberti S, Filardo G, Bordon J, Blasi F, Ramirez JA. Thrombocytopenia and thrombocytosis at time of hospitalization predict mortality in patients with community-acquired pneumonia. Chest 137(2):416-420; 2010.

Murphy EA, Francis ME. The estimation of blood platelet survival. II. Themultiple hit model. Thrombosis et Diathesis Haemorrhagica 25(1): 53-80; 1971.

Oldson D, Wentz J, Stricklin D. HENRE 2.0 technical reference manual. Tech. rep. DTRA-TR-15-070; 2015.

Palmer JL, Deburghgraeve CR, Bird MD, Hauer-Jensen M, Kovacs EJ. Development of a combined radiation and burn injury model. Journal of Burn Care and Research 32(2):317-323; 2011.

Pham TN, Cancio LC, Gibran NS. American Burn Association practice guidelines burn shock resuscitation. Journal of Burn Care and Research 29(1):257-266; 2008.

Pirkle JC, Gann DC. Restitution of blood volume after hemorrhage: mathematical description. The American Journal of Physiology 228(3):821-827; 1975.

Reisner AT, Heldt T. A computational model of hemorrhage and dehydration suggests a pathophysiological mechanism: Starling-mediated protein trapping. Heart and Circulatory Physiology 304(4):H620-H631; 2013.

Romero-Weaver AL, Kennedy AR. Comparison of two methods for the determination of the effects of ionizing radiation on blood cell counts in mice. International Journal of Biomedical Science 8(1):7; 2013.

Romero-Weaver AL, Wan XS, Diffenderfer ES, Lin L, Kennedy AR. Kinetics of neutrophils in mice exposed to radiation and/or granulocyte colony-stimulating factor treatment. Radiation Research 180(2):177-188; 2013.

SatyamitraM, Lombardini E, Graves J, Mullaney C, Ney P, Hunter J, Johnson K, Tamburini P, Wang Y, Springhorn JP, Srinivasan V. A TPO receptor agonist, ALXN4100TPO, mitigates radiation-induced lethality and stimulates hematopoiesis in CD2F1 mice. Radiation Research 175(6): 746-758; 2011.

Satyamitra M, Ney P, Graves J, Mullaney C, Srinivasan V. Mechanism of radioprotection by δ tocotrienol:pharmacokinetics, pharmacodynamics and modulation of signaling pathways. British Journal of Radiology 85:e1093-e1103; 2012.

Shaw A, Anderson J, Hayward A, Parkhouse N. Pathophysiological basis of burn management. British Journal of Hospital Medicine 52(11):583-587; 1994.

Singh VK, Brown DS, Kao TC. Tocopherol succinate: A promising radiation countermeasure. International Immunopharmacology 9(12):1423-1430; 2009.

Smetana K, Synek P, Mičánková M. The lymphocytic reaction to blood donation in the peripheral blood of healthy blood donors. Leipzig: Folia Haematologica 110(2):177-186; 1983.

Smirnova OA. Environmental radiation effects on mammals. New York: Springer; 2010.

Smirnova OA. Comparative analysis of the dynamics of thrombocytopoietic, granulocytopioetic, and erythropoietic system in irradiated humans: a modeling approach. Health Physics 103(6):787-801; 2012.

Smith F, Smith WW, Gonshery L, Grenan MM. Effect of immunity on resistance to infection in irradiated mice and rats. Experimental Biology and Medicine 87(1):23-26; 1954.

Starr T, Starr E. Biology: The unity and diversity of life. Lachina Publishing Services.

Stavem P, Brøgger, Devik F, Flatby J, van der Hagen CB, Henriksen T, Hoel PS, Høst H, Kett K, Petersen B. Lethal acute gamma radiation accident at Kjeller, Norway: Report of a case. Acta Radiologica: Oncology 24(1):61-63; 1985.

Stohlawetz P, Stiegler G, Jilma B, Dettke M, Höcker R, Panzer S. Measurement of the levels of reticulated platelets after plateletpheresis to monitor activity of thrombopoiesis. Transfusion 38(5):454-458; 1998.

Stricklin D. Overview of burn shock pathophysiology. ARA/HS-TN-13-001-A, ARA Technical note. Arlington, VA: Applied Research Associates; 2013.

StricklinD, Oldson D. An Overview of the Technical Basis for HENRE 2.0 Models. Tech. rep. DTRA-TR-15-071; 2015.

Sullivan LW, Adams WH, Liu YK. Induction of thrombocytopenia by thrombopheresis in man: patterns of recovery in normal subjects during ethanol ingestion and abstinence. Blood 49(2):197-207; 1977.

Summers, C, Rankin SM, Condliffe AM, Singh N, Peters M, Chilvers ER. Neutrophil kinetics in health and disease. Trends in Immunology 31(8):318-324; 2010.

Tølløfsrud S, Tønnessen T, Skraastad Ø, Noddeland H. Hypertonic saline and dextran in normovolaemic and hypovolaemic healthy volunteers increases interstitial and intravascular fluid volumes. Acta Anaesthesiologica Scandinavia 42(2):145-153; 1998.

Tough DF, Sprent J. Lifespan of lymphocytes. Immunologic Research 14(1):1-12; 1995.

Torres A, Bentley T, Bartels J, Sarkar J, Barclay D, Namas R, Constantine G, Zamora R, Puyana JC, Vodovotz Y. Mathematical modeling of posthemorrhage inflammation in mice: studies using a novel, computer-controlled, closed-loop hemorrhage apparatus. Augusta, Georgia: Shock 32(2):172-178; 2009.

Valentin J, Basic anatomical and physiological data for use in radiological protection: reference values. Annals of the ICRP 32(3-4):1-277; 2002.

Weisbach V, Friedlein H, Glaser A, Zingsem J, Zimmermann R, Eckstein R. The influence of automated platelet pheresis on systemic levels of hematopoietic growth factors. Transfusion 39(8):889-894; 1999.

Wentz J, Oldson D, Stricklin D. Mathematical models of human hematopoiesis following acute radiation exposure. Tech. rep. DTRA-TR-14-031; 2014.

Wentz J, Oldson D, Stricklin D. Models of hematopoietic dynamics following burn for use in combined injury simulations. Tech. rep. DTRA-TR-15-024; 2015.

Williams C. Successful assessment and management of burn injuries. Nursing Standard 23(32):53-62; 2009.

Yarmonenko SP. Radiation sickness in man. Radiobiology of Humans and Animals; 1988.

Section 6.

Abbreviations, Acronyms and Symbols

ARA	Applied Research Associates, Inc.
CSM	Coupled Starling Model
DTRA	Defense Threat Reduction Agency
Gy	Gray
HENRE	Health Effects from Nuclear and Radiological Environments
HSC	Hematopoietic stem cells
iNOS	Inducible nitric oxide synthase
MKs	Megakaryocytes
NETs	Neutrophil extracellular traps
NHP	Non-human primates
PBL	Percent of blood lost
TP	Thrombocytapheresis
TPO	Thrombopoietin
WBC	White Blood Cell
WMD	Weapons of mass destruction
% TBSA	Percent of total body surface area

Appendix A. Supplemental Tables

Table A-1. Human Thrombocytapheresis Data

Reference	Number of Donors
Dettke et al. 1998	11 males, 12 females
Fontana et al. 2011	At least 20 donors per group[a]
Lasky et al. 1981	7-33 donors
Stohlawetz et al. 1998	13 donors on average[b]
Sullivan et al. 1977	2
Weisbach et al. 1999	21 male donors

[a]Donors were split into three groups based on previous donation yields: double, triple and quadruple-unit
[b]Donors were split into two groups: first time and repeat donors

We used the same approach for the human and murine models to optimize the radiation-induced demargination parameters. The non-dimensional models were compared to normalized experimental data and the error of each simulation was quantified using a cost function, defined as the average residual between the simulated and experimental data. The global search algorithm, differential evolution, was used to find an optimal parameter set of values for a_r, b_r, k_r and A_r. All computations were performed with the statistical computing environment R (R Core Team 2013), and differential evolution was performed with the DEoptim function in the Global Optimization by Differential Evolution library (DEoptim) (Ardia et al. 2015). Table A-2 provides the parameter values resulting from optimization.

Table A-2. Radiation-Induced Granulocyte Demargination Parameters

Parameter	Biological Meaning	Human Value	Murine Value
a_r	Determines duration of radiation effect on margination ratio	0.35 d^{-1}	0.222 d^{-1}
b_r*	Determines max radiation effect on margination ratio	0.334	0.186
k_r	Determines demargination dependency on radiation dose	0.336	69.055
A_r*	Determines demargination dependency on radiation dose	1	0.25

*b_r and A_r converged to boundary values during optimization

We used the same approach to determine murine hemorrhage-induced demargination parameters as was used to determine radiation-induced demargination parameters. We optimized the ability

of the murine model to simulate hemorrhage data from Gaylor et al. 1969 using the methods described above. Without human data, we decided to extrapolate human parameters based on the radiation-induced demargination of the human and murine models, and the hemorrhage-induced demargination of the murine model. More specifically, we assumed that the scaling factor between a_h and a_r is the same between humans and mice ($\frac{a_{h,h}}{a_{r,h}} = \frac{a_{h,m}}{a_{r,m}} \approx 4.3$). This assumes the relaxation rates of demargination between hemorrhage and radiation are scaled in the same way. $b_{h,m}$ converged to its boundary value during optimization. This boundary value was set to ensure that no more than 100% of circulating granulocytes can be demarginated at any given time. We assume the same is true for the human model, setting $b_{h,h}$ to its maximum value. Finally, we assume that the human and murine demargination dependence of PBL (controlled by k_h and A_h) is equal, and thus set $k_{h,h} = k_{h,m}$ and $A_{h,h} = A_{h,m}$.

Table A-3. Hemorrhage-Induced Granulocyte Demargination Parameters

Parameter	Biological Meaning	Human Value (Extrapolated)	Murine Value (Optimized)
a_h	Determines duration of hemorrhage effect on margination ratio	1.505 d^{-1}	0.962 d^{-1}
b_h	Determines max hemorrhage effect on margination ratio	1	3*
k_h	Determines demargination dependency on PBL	0.1	0.1
A_h	Determines demargination dependency on PBL	0.1	0.1

*b_h converged to its boundary value during optimization for the murine model

Table A-4. Human Optimization Data for Radiation-Induced Granulocyte Demargination

Incident/Subject	Reference	Dose (Gy)	Baseline ($10^3 \mu L^{-1}$)
Los Alamos 1945–2	Hempelmann et al. 1952	0.12	4.102[a]
UT CARL 1971	Andrews et al. 1961*	2.6	4.102[a]
Argonne 1952–I	Bond et al. 1965	1.5	4.102[a]
Y-12 1958–B	Andrews et al. 1961*	2.97	4.102[a]
Y-12 1958–C	Andrews et al. 1961*	3.73	4.102[a]
Y-12 1958–A	Bond et al. 1965	4.02	4.102[a]
Vinca 1958–B	Jammet et al. 1959	3.51	4.102[a]
Vinca 1958–H	Jammet et al. 1959	4.37	4.102[a]
Vinca 1958–M	Jammet et al. 1959	5.74	4.102[a]
Vinca 1958–G	Jammet et al. 1959	5.35	4.102[a]
Vinca 1958–D	Jammet et al. 1959	5.40	4.102[a]
Vinca 1958–V	Jammet et al. 1959	3.11	4.102[a]
Yarmonenko 1988–Z	Yarmonenko 1988	9.8	4.102[a]
Cancer patients 1958–mean of 18	Miller et al. 1958	1.0	6.22[b]
Cancer patients 1958–mean of 12	Miller et al. 1958	1.5	6.99[b]
Cancer patients 1958–mean of 30	Miller et al. 1958	2.0	8.13[b]

[a]Mean granulocyte concentration observed in humans (Valentin 2002).
[b]Mean of pre-radiation data points.
*Data provided by Ron Goans.

Table A-5. Human Validation Data for Radiation-Induced Granulocyte Demargination

Incident/Subject	Reference(s)	Dose (Gy)	Baseline ($10^3 \mu L^{-1}$)
Brescia 1975	Mettler 2001	12	4.102[a]
Kjeller 1982	Stavem et al. 1985 Mettler 2001	22.5	4.102[a]
Lockport 1960–A	Bond et al. 1965 Howland et al. 1960	3	5.398[b]
Lockport 1960–B	"	3	5.398[b]
Los Alamos 1946–4	Hempelmann et al. 1952	3.6	5.32[b]
Los Alamos 1946–6	Hempelmann et al. 1952	1.6	4.35[b]
Los Alamos 1946–7	Hempelmann et al. 1952	1.1	4.102[a]
Los Alamos 1946–8	Hempelmann et al. 1952	0.65	3.22[b]
Los Alamos 1946–9	Hempelmann et al. 1952	0.47	4.2[b]
Los Alamos 1946–10	Hempelmann et al. 1952	0.37	5.12[b]
Marshallese 1954	Bond et al. 1965	1.68	4.102[a]
Mol 1965	Mettler 2001	5.5	4.102[a]
Sarov 1963	Mettler 2001	5.5	4.102[a]
Shanghai 1990	Mettler 2001	12	4.102[a]
Tokai-mura 1999–A	Hirama et al. 2003 Mettler 2001	20	4.102[a]
Tokai-mura 1999–B	"	7.4	4.102[a]
Y-12 1958–E	Bond et al. 1965 Mettler 2001 Andrews et al. 1961* Kerr and Tankersley 2006	2.59	4.102[a]

[a]Mean granulocyte concentration observed in humans (Valentin 2002).
[b]Mean of pre-radiation data points.
*Data provided by Ron Goans.

Table A-6. Murine Optimization Data for Radiation-Induced Granulocyte Data

Reference	Dose (Gy)	Baseline ($10^3 \mu L^{-1}$)
Brecher and Endicott 1948	0.384	1.6[a]
Davis et al. 2010	7.5	0.473[a]
Ghosh et al. 2012	6	2.489[a]
Kulkarni et al. 2013	8	2.596[b]
Palmer et al. 2011	5	2.422[b]
Romero-Weaver and Kennedy 2012	2	n/a[c]
Romero-Weaver et al. 2013	2	n/a[c]
Satyamitra et al. 2011	7	1.175[b]
Satyamitra et al. 2012	7	0.91[a]
Singh et al. 2009	3, 7	0.774[b]
Smith et al. 1954	4.56, 5.76	1.231[a]

[a]Mean granulocyte concentration of control.

[b]Mean of post radiation controls; controls given for each time point.

[c]Data presented as % of control.

Appendix B. Supplemental Figures

B-1. Human Thrombocytapheresis Experiments

We used the thrombocytapheresis (TP) data provided in Table A-1 to validate the human thrombopoiesis model in the context of hemorrhage. Simulations of these experiments are provided in Figure B-5 - Figure B-13 (human data) and Figure B-14 - Figure B-17 (murine data).

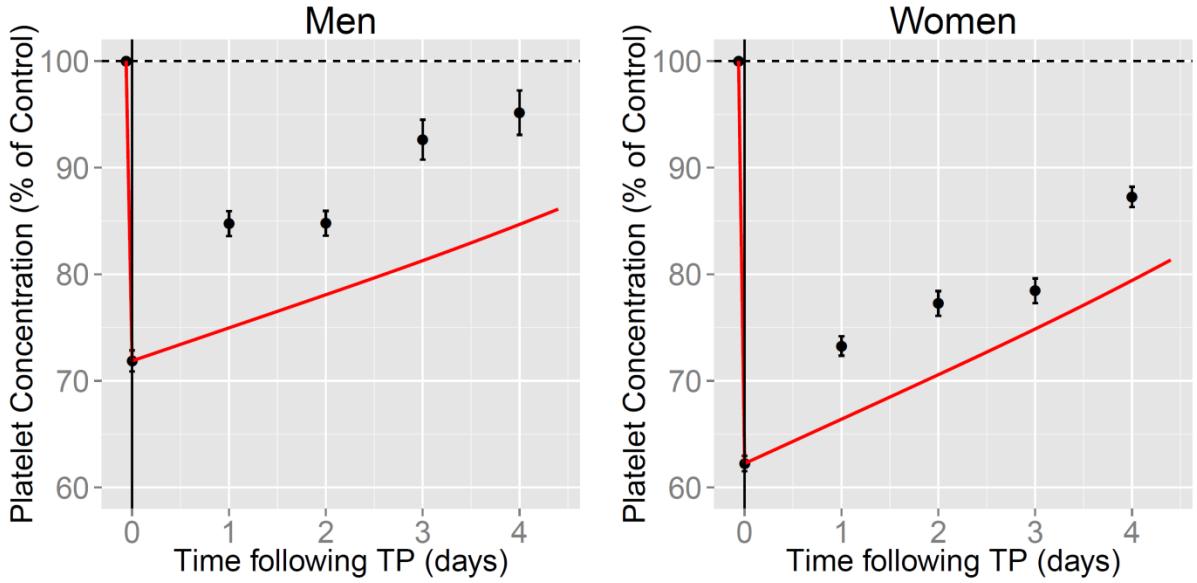

Figure B-1. Simulation of a human TP study (Dettke 1998) with the thrombopoiesis model

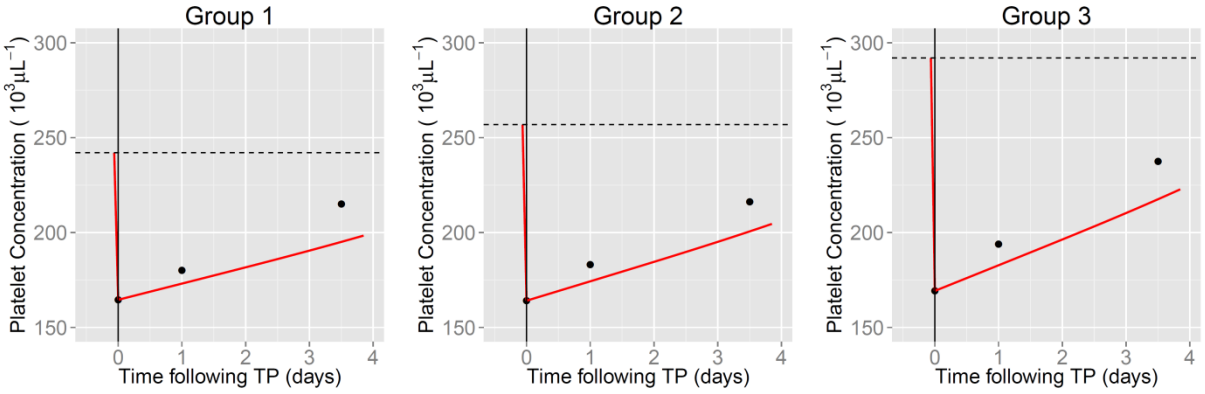

Figure B-2. Simulation of a human TP study (Fontana 2011) with the thrombopoiesis model

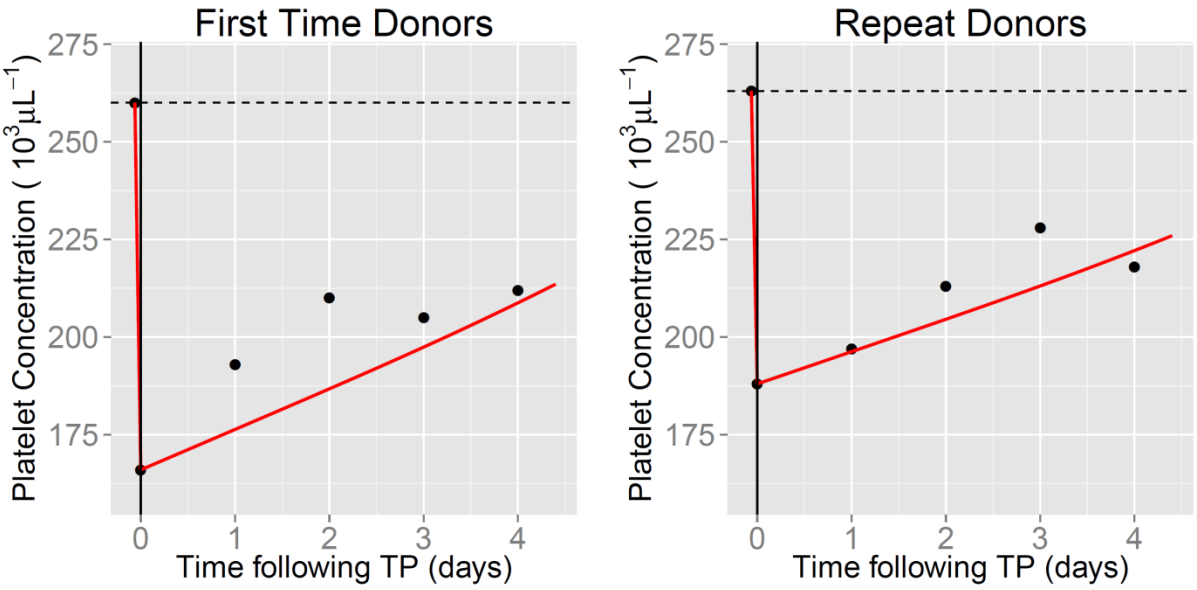

Figure B-3. Simulation of a human TP study (Stohlawetz 1998) with the thrombopoiesis model

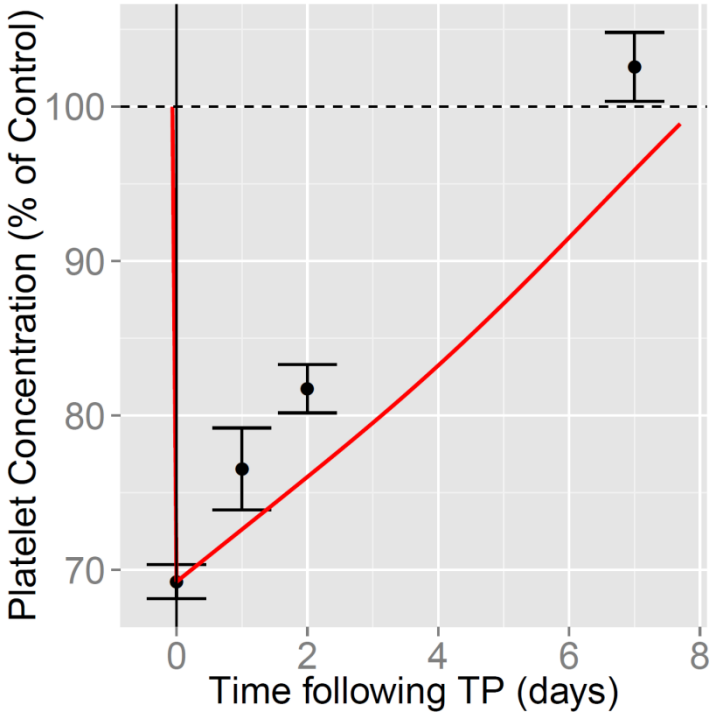

Figure B-4. Simulation of a human TP study (Weisbach 1999) with the thrombopoiesis model

B-2. Human Radiation-Induced Granulocyte Demargination

We used the data provided in Table A-4 and Table A-5 to optimize and validate the human radiation-dependent granulocyte demargination parameters. Simulations of these experiments are provided in Figure B-5 to Figure B-13.

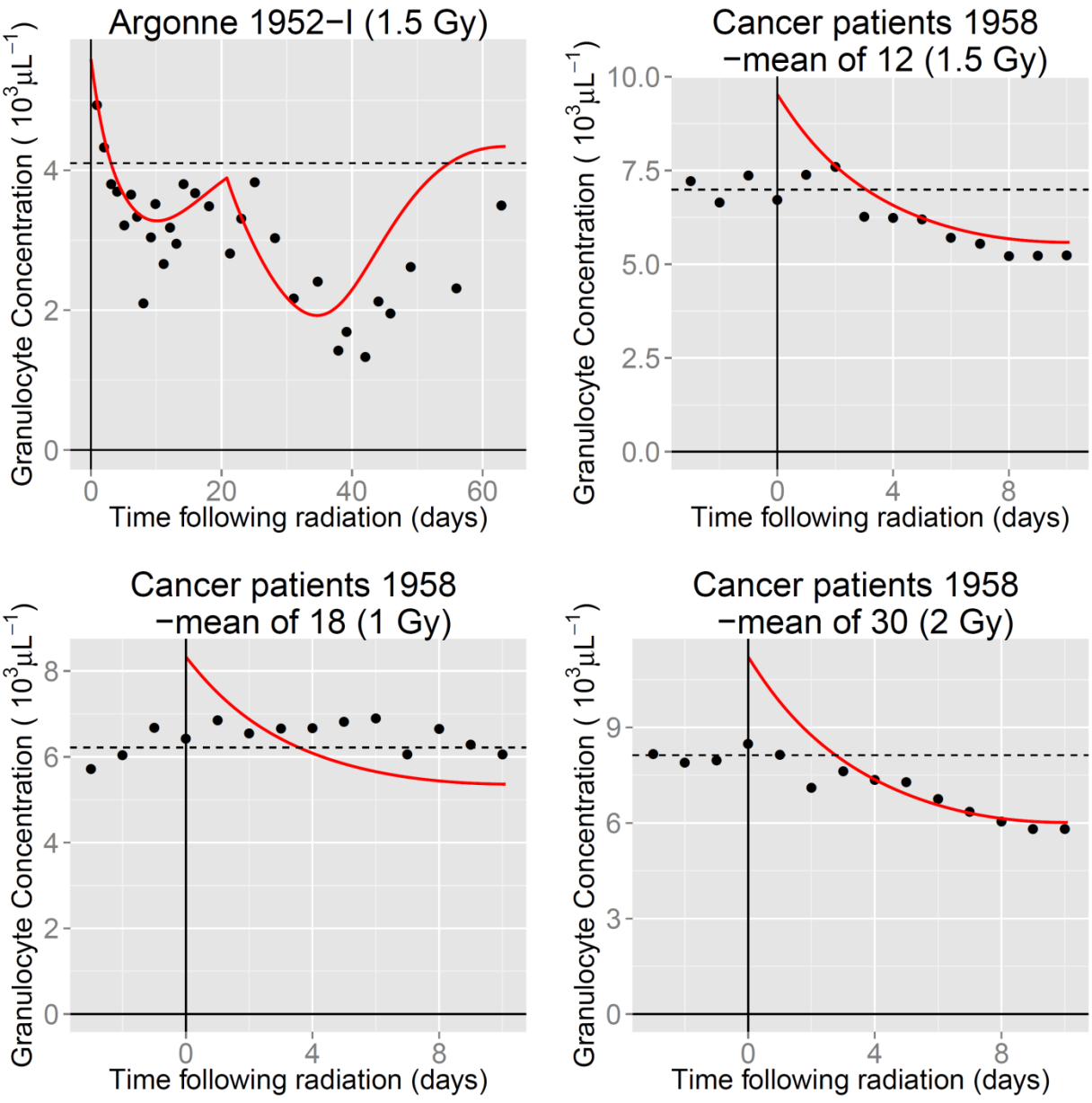

Figure B-5. Human granulocyte data used for optimization of radiation-induced demargination parameters (1 of 4)

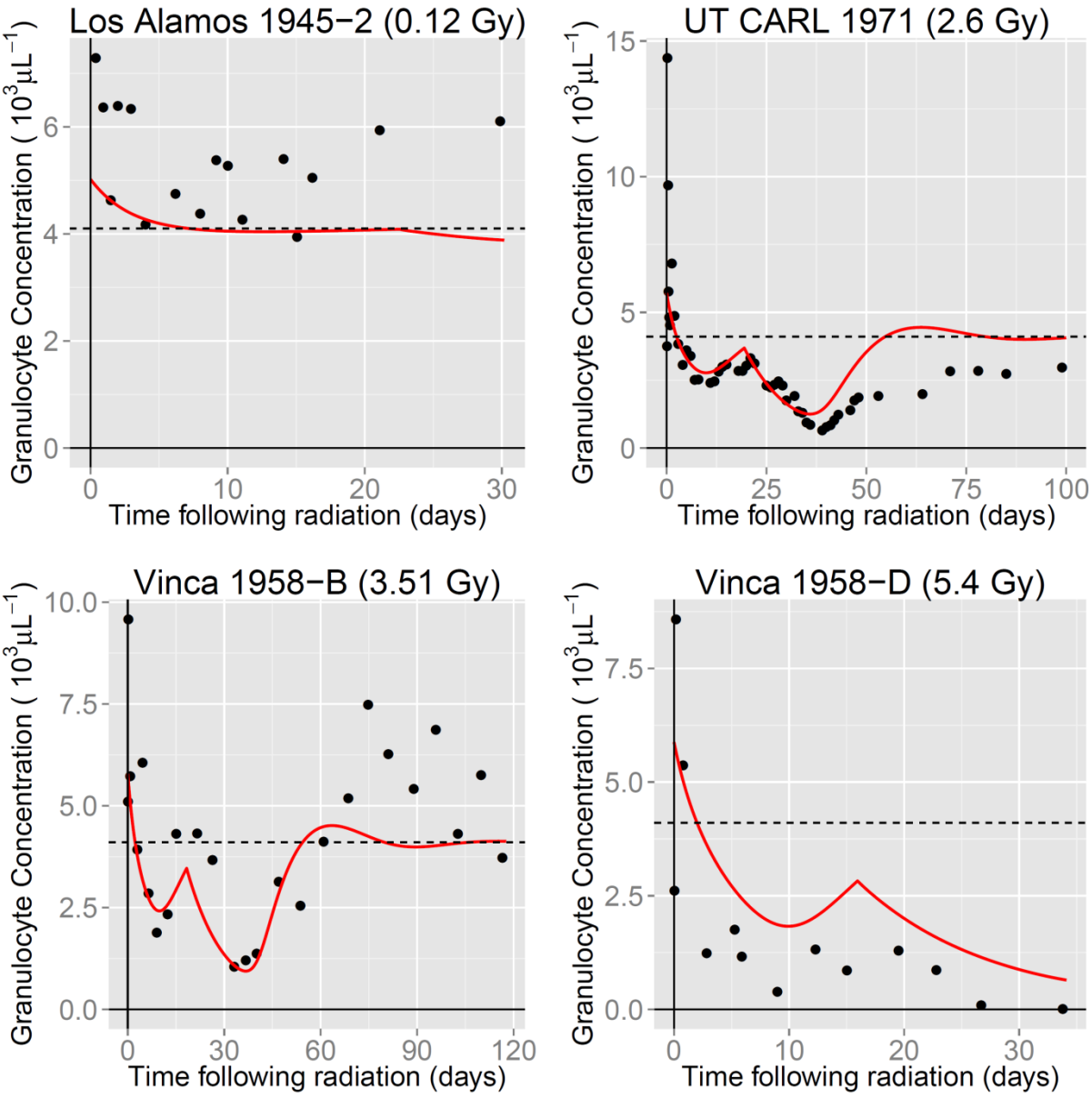

Figure B-6. Human granulocyte data used for optimization of radiation-induced demargination parameters (2 of 4)

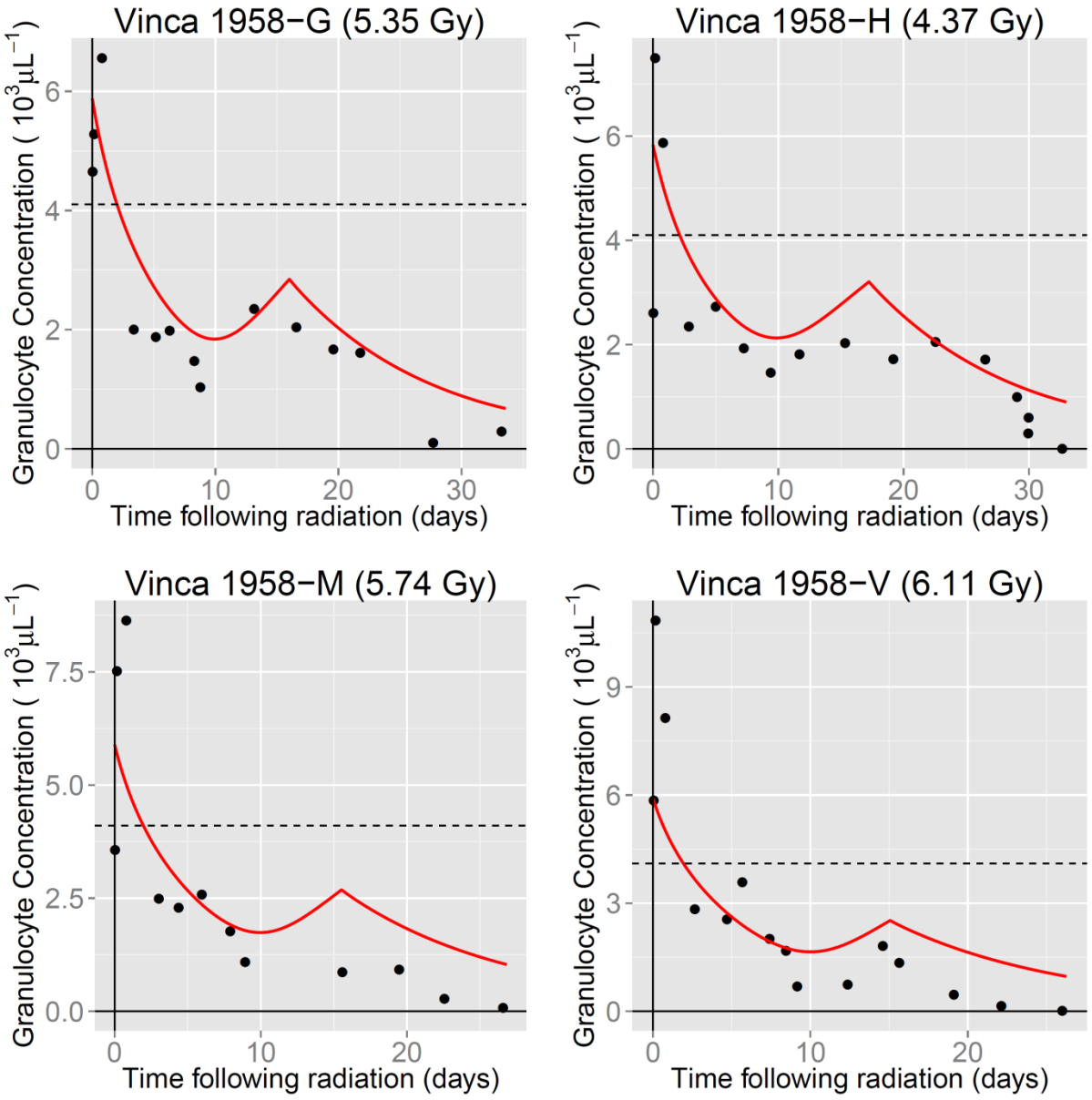

Figure B-7. Human granulocyte data used for optimization of radiation-induced demargination parameters (3 of 4)

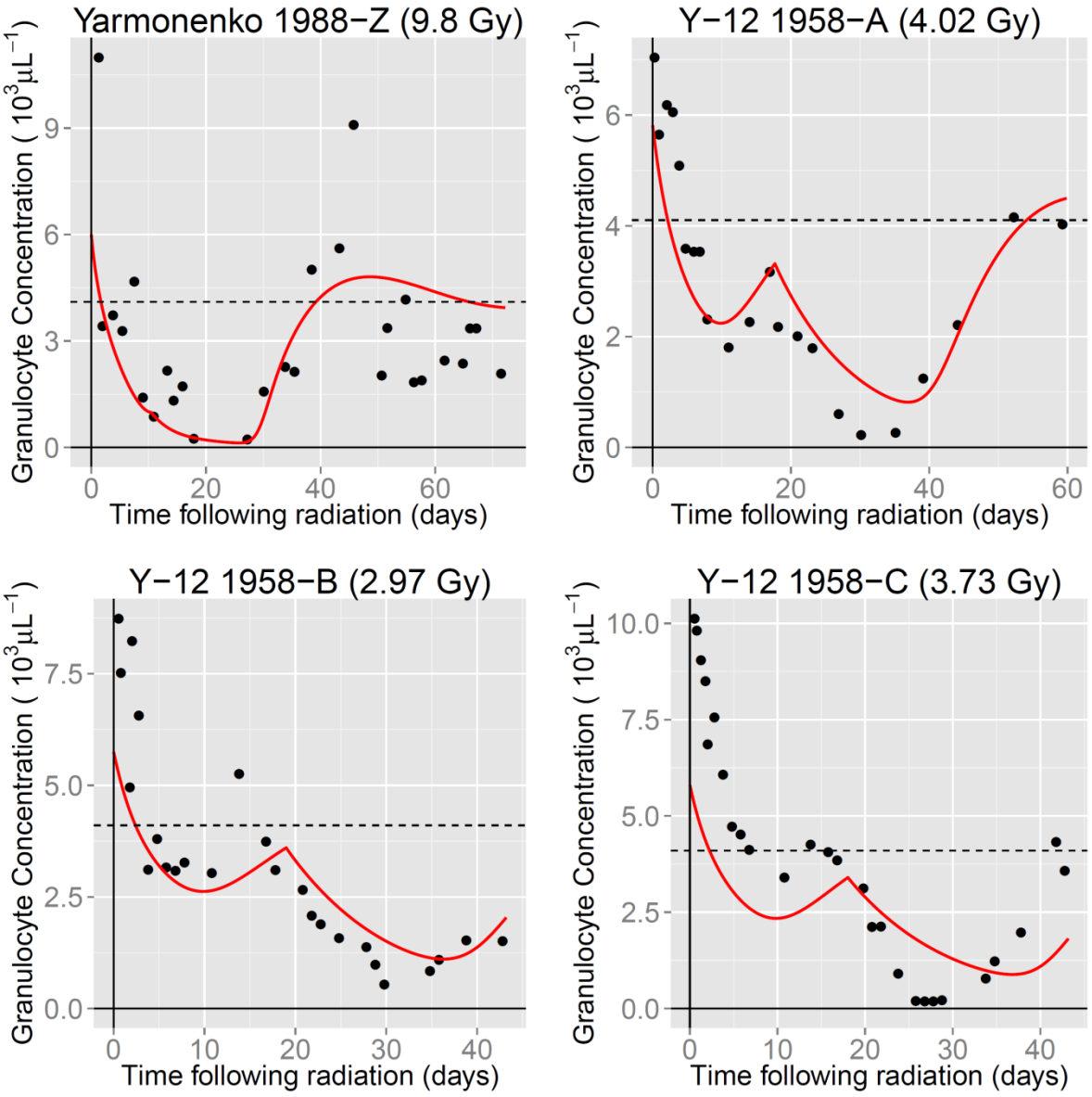

Figure B-8. Human granulocyte data used for optimization of radiation-induced demargination parameters (4 of 4)

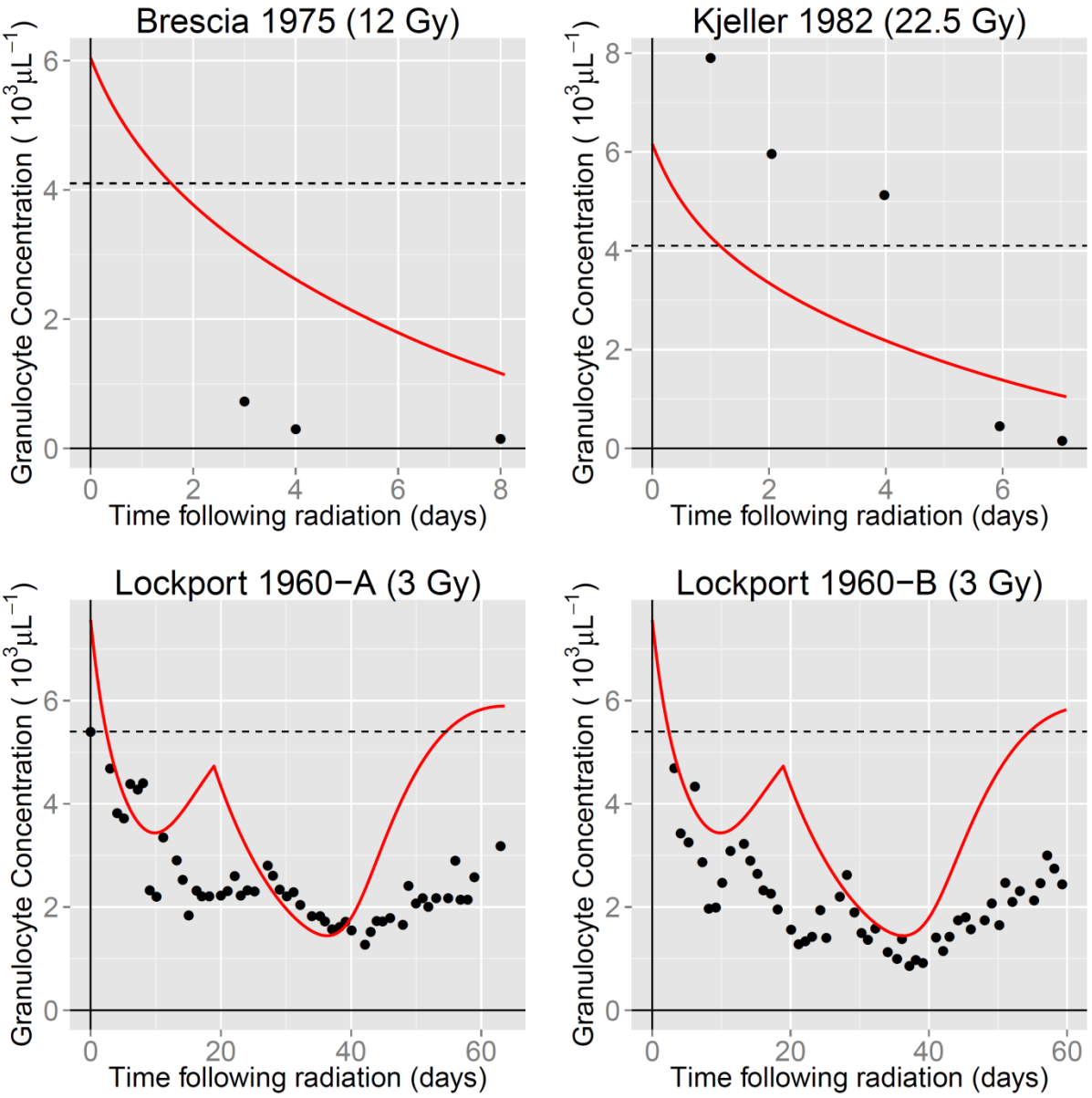

Figure B-9. Human granulocyte data used for validation of radiation-induced demargination parameters (1 of 5)

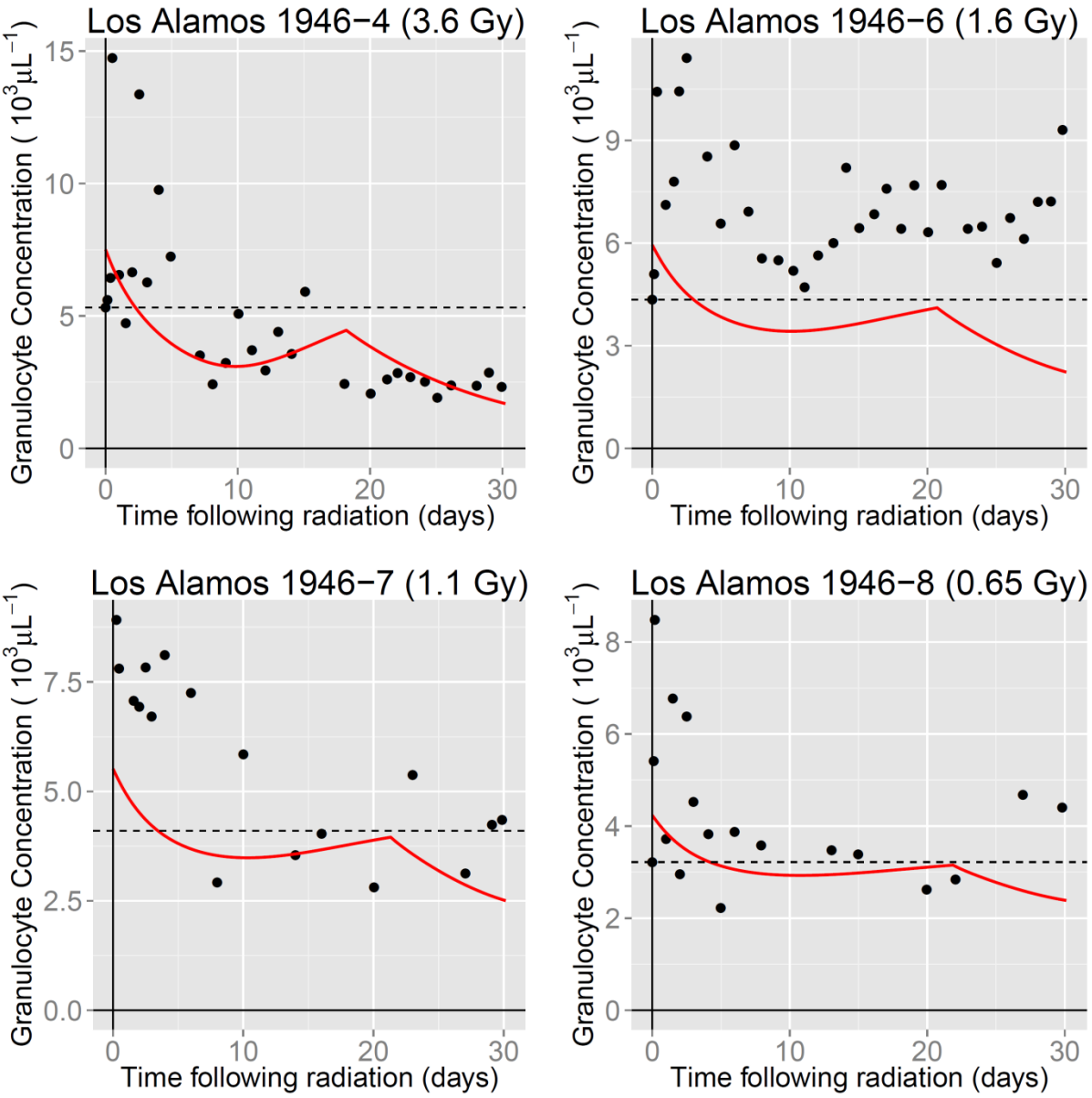

Figure B-10. Human granulocyte data used for validation of radiation-induced demargination parameters (2 of 5)

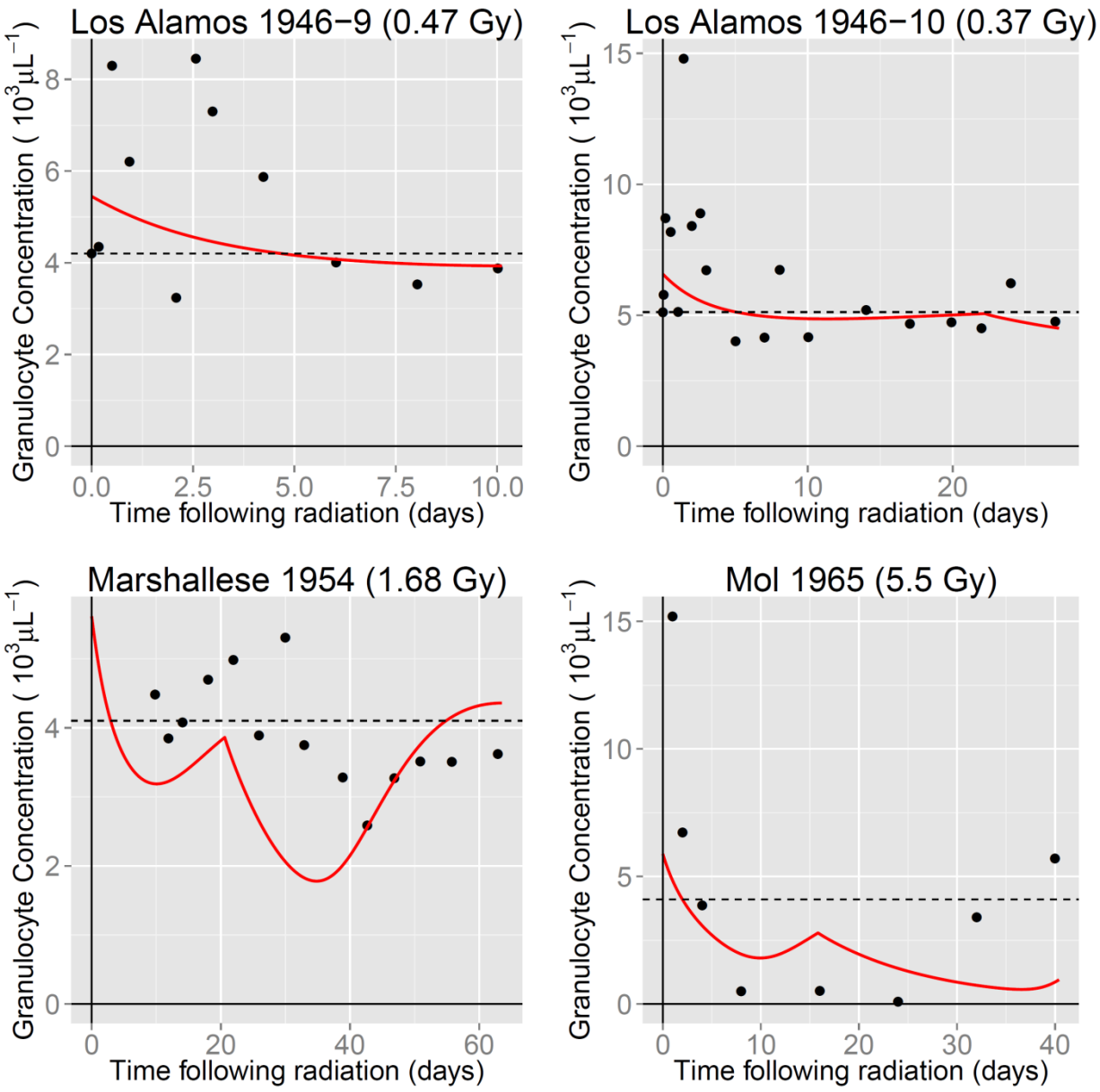

Figure B-11. Human granulocyte data used for validation of radiation-induced demargination parameters (3 of 5)

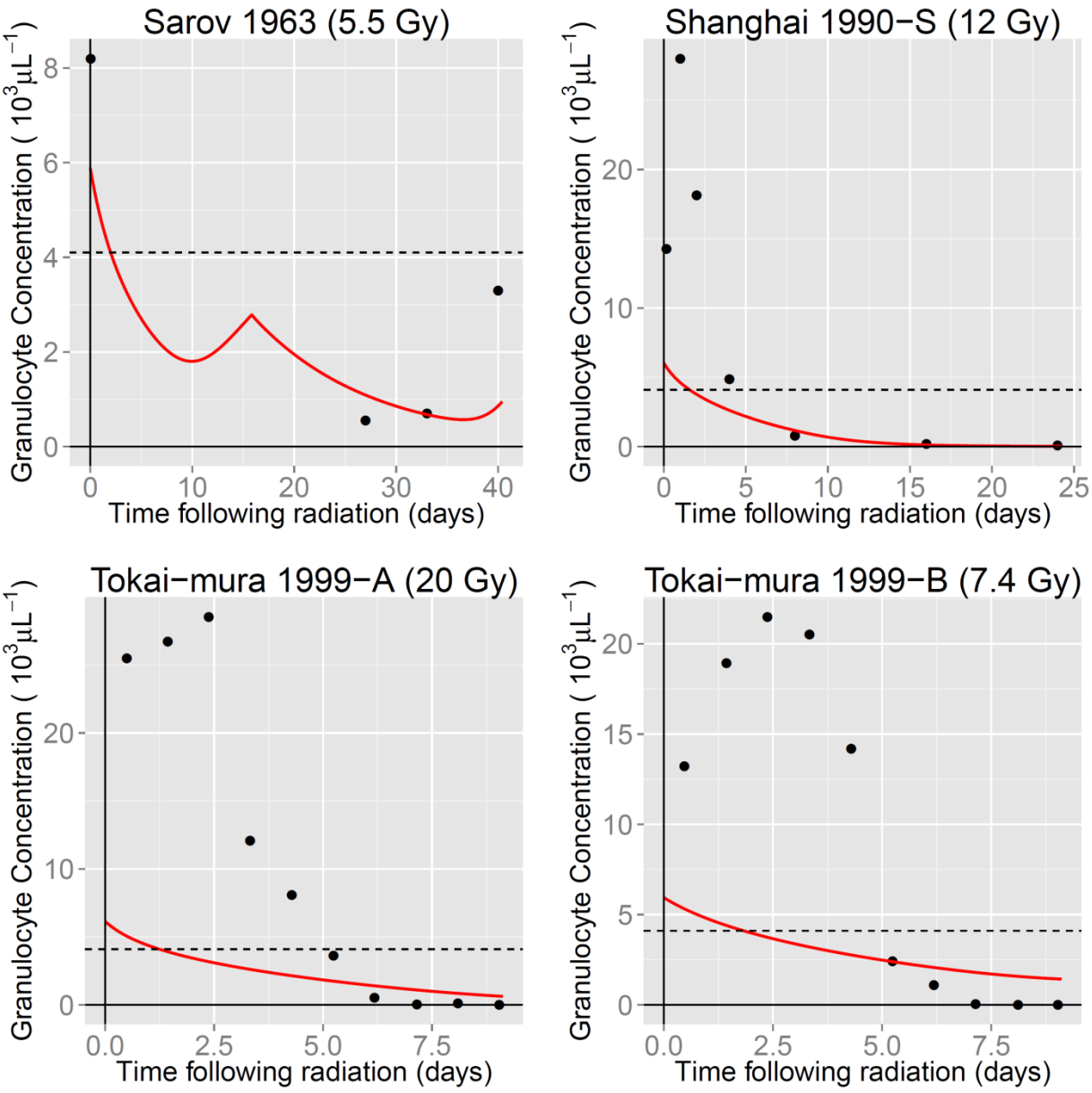

Figure B-12. Human granulocyte data used for validation of radiation-induced demargination parameters (4 of 5)

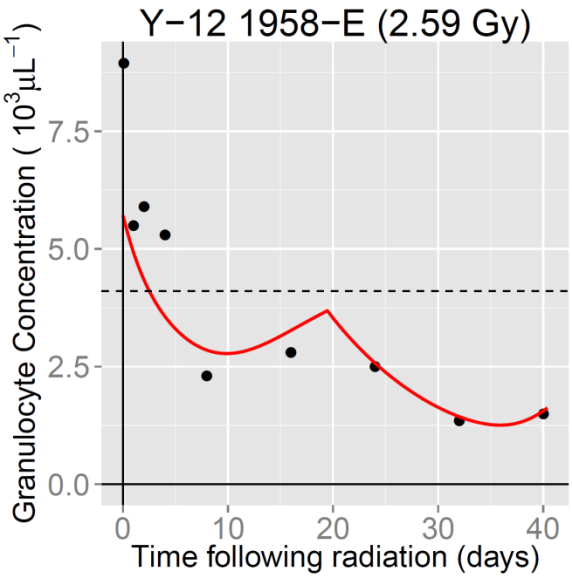

Figure B-13. Human granulocyte data used for validation of radiation-induced demargination parameters (5 of 5)

B-3. Murine Radiation-Induced Granulocyte Demargination

We used the data provided in Table A-6 to optimize the murine radiation-dependent granulocyte demargination parameters. Simulations of these experiments are provided in Figure B-14 to Figure B-17.

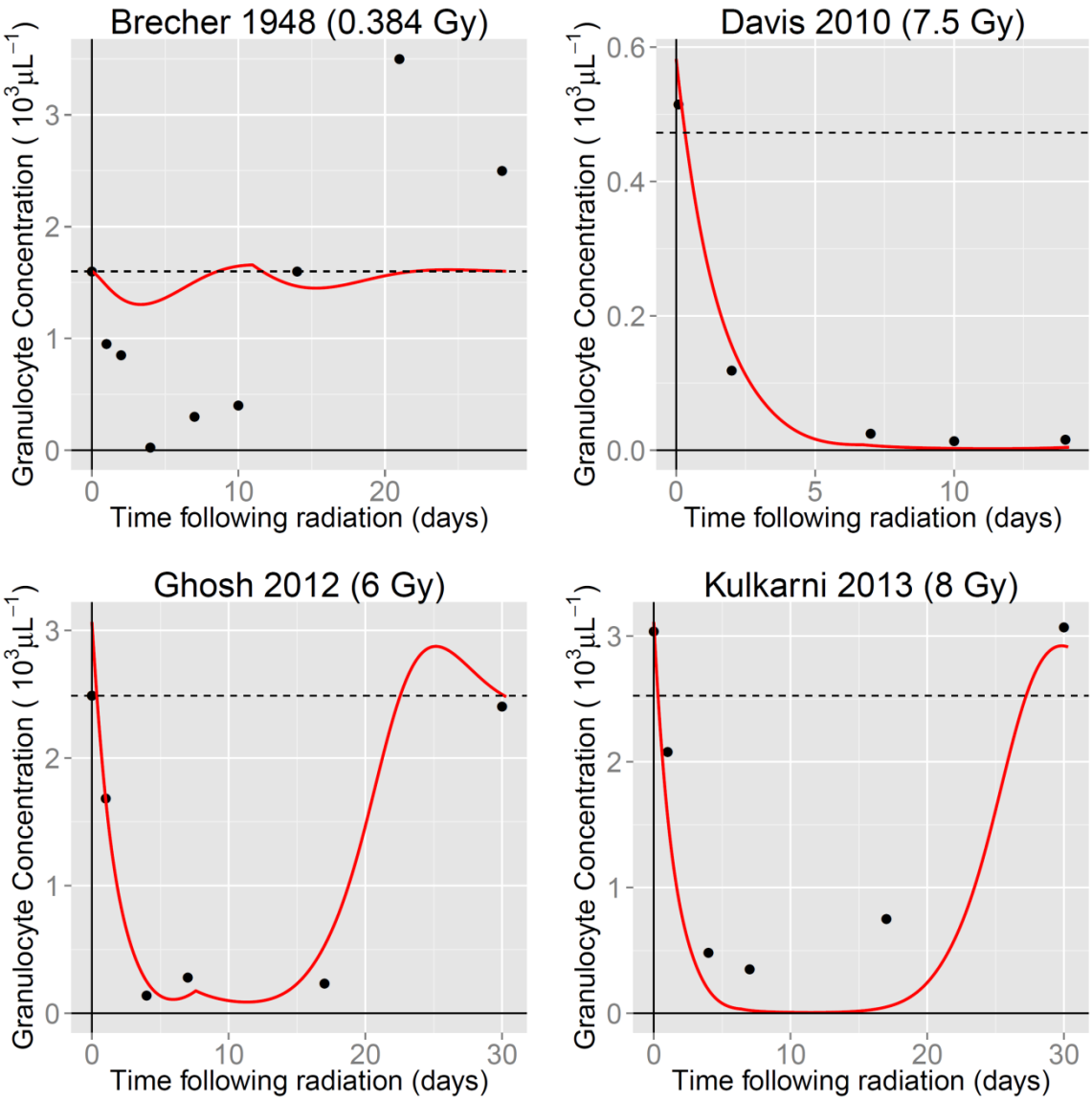

Figure B-14. Murine granulocyte data used for optimization of radiation-induced demargination parameters (1 of 4)

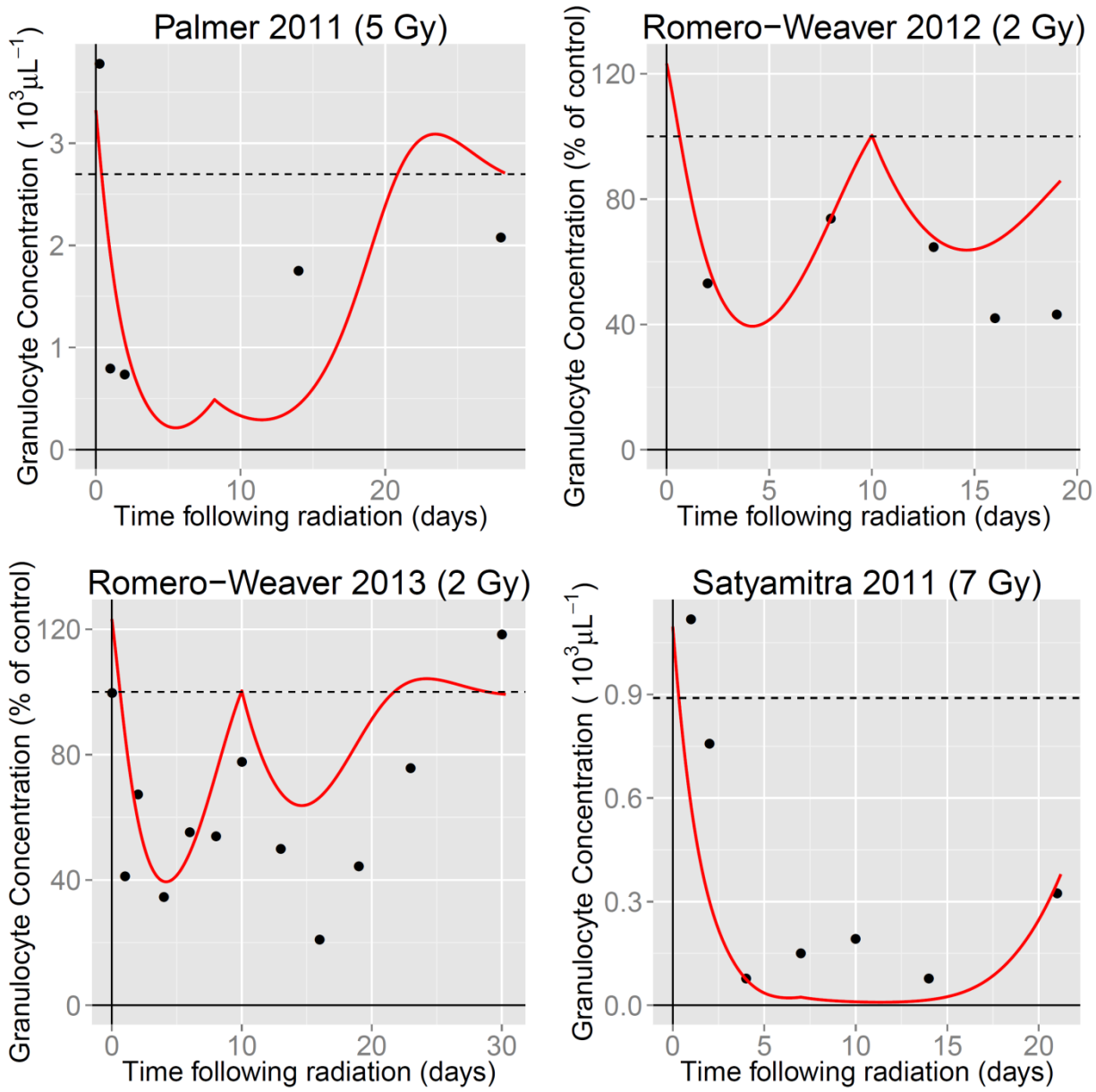

Figure B-15. Murine granulocyte data used for optimization of radiation-induced demargination parameters (2 of 4)

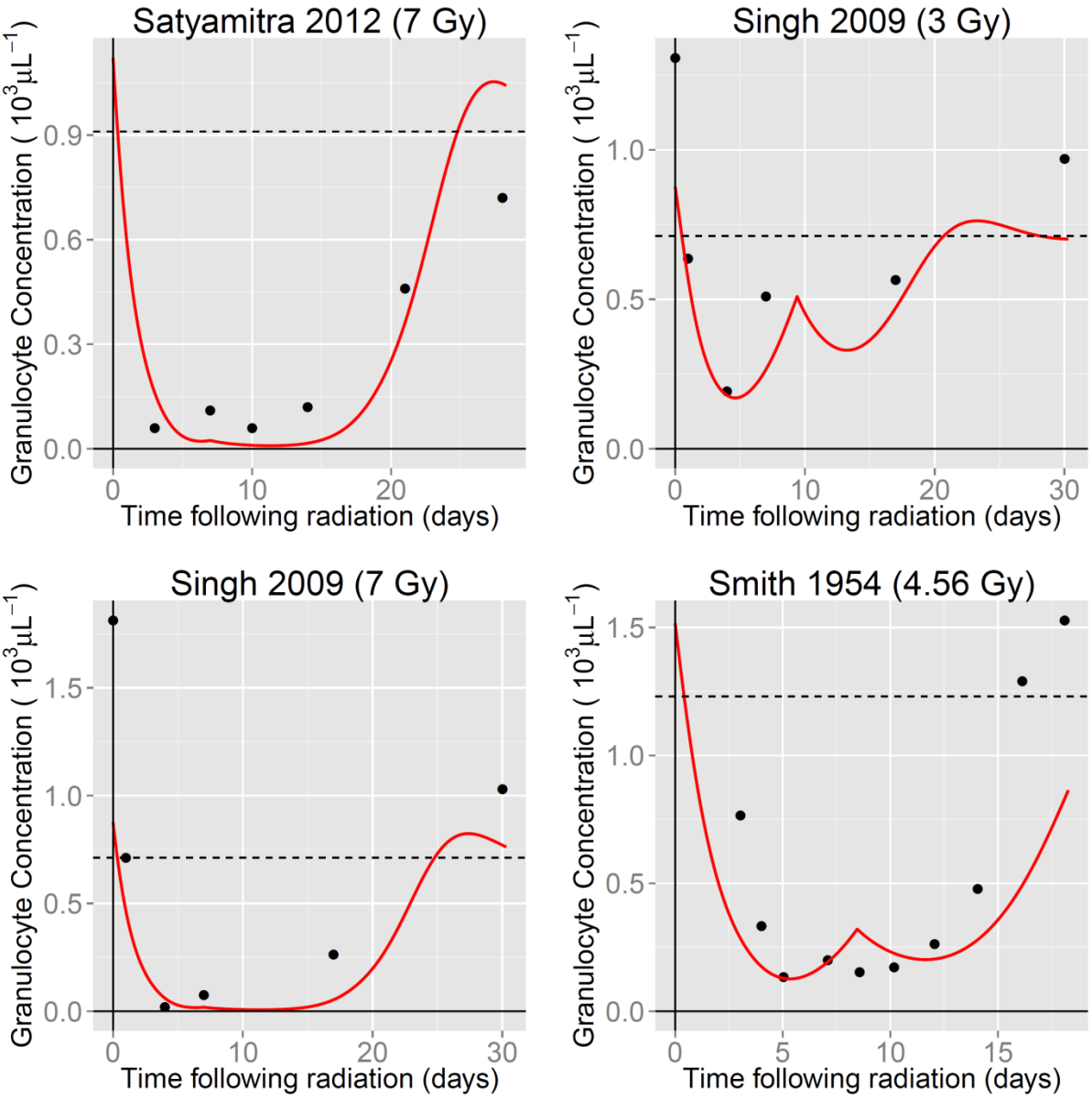

Figure B-16. Murine granulocyte data used for optimization of radiation-induced demargination parameters (3 of 4)

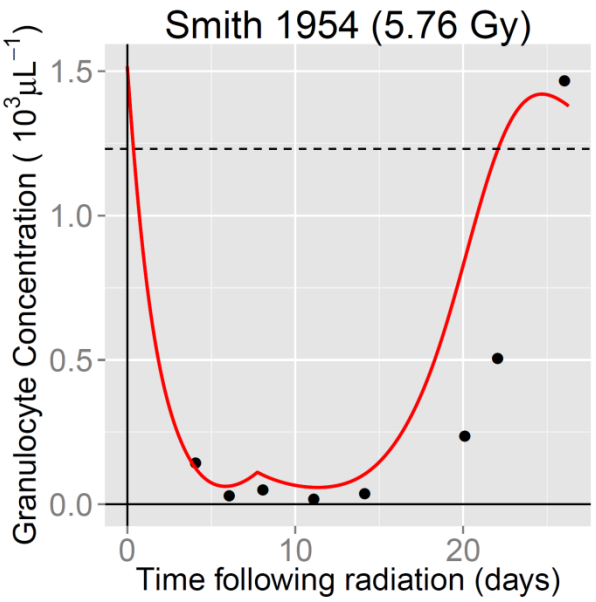

Figure B-17. Murine granulocyte data used for optimization of radiation-induced demargination parameters (4 of 4)